Reliable DC Shipboard Power Systems - Design, Assessment, and Improvement

Van Der Sande, Robin; Shekhar, Aditya; Bauer, Pavol

DOI
10.1109/OJIES.2025.3532095

Publication date
2025

Document Version
Final published version

Published in
IEEE Open Journal of the Industrial Electronics Society

IEEE Open Journal of the
Industrial Electronics Society

Received 3 December 2024; accepted 12 January 2025. Date of publication 20 January 2025;
date of current version 14 February 2025. The review of this article was arranged by Associate Editor Oscar Lucia.

Digital Object Identifier 10.1109/OJIES.2025.3532095

Reliable DC Shipboard Power Systems—Design, Assessment, and Improvement

ROBIN VAN DER SANDE (Student Member, IEEE), ADITYA SHEKHAR (Member, IEEE), AND PAVOL BAUER (Senior Member, IEEE)

Electrical Sustainable Energy Department, Delft University of Technology, 2628 CD Delft, The Netherlands

CORRESPONDING AUTHOR: ROBIN VAN DER SANDE (e-mail: R.P.J.vanderSande@tudelft.nl).

This work was supported by the Dutch Research Council (NWO) through the Survivable DC Power Systems for Ships Project under Grant KICH1.VE02.20.007.

ABSTRACT Targeting a climate-neutral maritime sector drives the adoption of the all-electric ship (AES). While AESs can utilize both ac and dc shipboard power systems (SPS), a dc system offers advantages in efficiency, power density, and source synchronization. However, the enhanced network complexity of dc grids combined with the high penetration of power electronic devices and harsh environmental conditions can compromise the system's reliability. Therefore, this article provides an overview of the reliability aspect of dc-SPSs, addressing the power system design, adequacy assessment, and reliability improvement. First, the performance tradeoffs associated with the SPS design are examined, revealing how changes in the power system topology and dc bus structure impact the vessel's reliability along with other performance parameters. Second, a hierarchical reliability model framework is proposed for the adequacy assessment of dc-SPSs, considering the reliability from the component level up to the system level. To determine the system-level reliability, multiple probabilistic methods, including simulation and analytical models, are compared using a propulsion subsystem example. Finally, an overview of the reliability improvement strategies is provided, addressing methods at the system, device, and component level. These three topics combined aim to provide guidance in the design of future reliable dc-SPSs.

INDEX TERMS DC systems, Monte Carlo (MC), reliability, shipboard power systems (SPS).

NOMENCLATURE

AES	All-electric ship.
BAAH	Breaker-and-a-half.
CB	Circuit breaker.
CI	Confidence interval.
COTS	Components off-the-shelf.
ESS	Energy storage system.
EENS	Expected energy not supplied.
FPS	Fault protection system.
FTA	Fault tree analysis.
HEW	High energy weapon.
IPS	Integrated power system.
LOLE	Loss of load expectation.
MC	Monte Carlo.
MCS	Minimal cut sets.
MMC	Modular multilevel converter.
MTBF	Mean time between failures.
MTBSI	Mean time between service interruptions.
MTTF	Mean time to failure.
MTTR	Mean time to repair.
MVDC	Medium voltage dc.
PCM	Power conversion module.
PE	Power electronic.
PGM	Power generation module.
PLM	Power load module.
QoS	Quality of service.
RBD	Reliability block diagram.
RV	Random variable.
SPS	Shipboard power system.

I. INTRODUCTION

In 2008, the maritime sector emitted over 1.1 billion tones of CO_2 accounting for 3.5% of the global emissions that year [1]. If the sector decides to postpone further efforts to combat climate change, its CO_2 share may rise to 17% by the year 2050 [2], [3]. However, following the 2023 GHG strategy of the International Maritime Organization, emission levels of international shipping are aimed to be cut by at least 70% in 2040, reaching net-zero around 2050 [4]. Pursuing this goal presents a massive challenge for the maritime sector, requiring both improvements in vessel efficiency and a transition from fossil fuels to renewable alternatives [3], [5].

A commonly proposed solution for addressing this challenge is the AES. An AES is a vessel that relies entirely on electricity to power its service and propulsion loads. The basis of an AES is the SPS, which serves as the interconnecting grid between the electric loads and the PGM, combining the functionality of the traditional split electric power and propulsion power system [6]. Because of its structure, a SPS offers efficient methods for integrating renewable energy sources in the vessel's propulsion system, utilizing technologies such as fuel cells and port charging [7], [8], [9], [10]. In addition, using a SPS can enhance the vessel's efficiency and allow for improved automation in energy management, power flow control, and fault protection [11], [12]. Together, these features make the AES a promising technology for establishing a future sustainable maritime sector. Further advantages of the AES over a mechanical propulsion alternative include the following.

1) Enhanced vessel efficiency via more efficient operation and improved management of prime movers [13], [14].
2) Lower life-cycle cost through reduced fuel consumption, lower maintenance requirements, and improved automation [11], [12], [15], [16].
3) Enhanced vessel maneuverability and position-keeping ability with faster electrical motors and straightforward integration of podded propulsion [12], [14], [17].
4) Simpler ESS integration, allowing for peak shaving and emission-free operation [14], [18].
5) Higher power system design flexibility, trough reduced location restrictions for components and easier integration of modularity, redundancy, and reconfigurability, improving the system reliability and survivability [6], [12], [15], [19], [20], [21].

Although the SPS provides many advantages over the mechanical propulsion alternative, its design comes with a set of challenges. Compared to land-based power grids, a SPS has severe restrictions on the size and weight of its components. Meanwhile, the SPS architecture must adapt to the structural arrangement of the vessel, increasing its design complexity. Moreover, a SPS is exposed to a severely fluctuating load profile, where loads like positioning thrusters impose rapid changes in the power demand, reducing the system stability and efficiency [22].

The concept of using electricity onboard ships dates back over a century. In 1880, the *SS Columbia* was the first vessel to use a dc system to power its lights. Later, in 1903, a tanker vessel named *Vandal* was the first ship equipped with diesel–electric propulsion, where three 500 V dc generators were used to provide 290 kW of propulsion power. In 1912, the first electric-propulsion naval vessel, named the *USS Jupiter*, was constructed. This ship contained a single 5000 kW ac steam turbo-generator that powered two induction motors. Because of its success, many US Navy vessels, including the *USS New Mexico*, *USS West Virginia*, and *USS Lexington* adopted the turbo-electric propulsion. In the years that followed, diesel engines took over as prime movers, leading to a significant decline in the use of electric propulsion. Nevertheless, with the development of semiconductor technology in the 1980 s and the growing emphasis on fuel efficiency, the *Queen Elizabeth II* (1984) was refitted with a diesel–electric integrated propulsion system using ac drives to control two 44 MW motors. Since then, ac-SPSs were commonly used to power both naval and commercial vessels. However, with the continued advancement in PE, new technologies like the solid-state dc breakers made dc-SPSs more appealing. In 2016, the *USS Zumwalt* was therefore constructed with a 1 kV dc grid to power its service loads. Since then, other navies, including the Royal Netherlands Navy (*ASWF*), German Navy (*F126*), and Spanish Navy (*BAM-IS*), have also opted for a shipboard dc grid. In addition to these naval vessels, dc-SPSs have found their way into commercial vessels. The *Dina Star*, launched in 2013, was the first vessel to be equipped with ABB's onboard dc grid. A list of other vessels commissioned with a dc-SPS is provided in Table 1.

TABLE 1. Overview of Commissioned Vessels With a dc-SPS, Their System Provider, and the Operation Parameters

Name:	Type:	Year:	System provider:	V_{dc}	$P_r \approx$
Dina Star	Supply	2013	ABB: Onboard DC	1000V	10MW
MS Amera	Cruise	2024	ABB: Onboard DC	1000V	18MW
Ulsan Taehwa	Ferry	2022	HD Hyundai	LVDC	4MW
OV Ryvingen	Utility	2018	Kongsberg	LVDC	2MW
Vittorio Morace	Ferry	2023	MTU: PropulsionPack	LVDC	1MW
Kommandøren	Ferry	2018	NES: Odin's EYE	LVDC	2MW
Shen Kuo	Research	2018	SES-Tech S-DE	1050V	2MW
Victoria Sabrina	Cruise	2020	SES-Tech: S-Ren.	1050V	5MW
Edda Freya	Constr.	2016	Siemens: BlueDrive	880-1050	18MW
Bastø Electric	Ferry	2021	Siemens: BlueDrive	880-1050	7MW
Viking Princess	Supply	2018	The Switch: DC-Hub	LVDC	6MW
Aurora Botnia	Ferry	2021	WE Tech & Danfoss	LVDC	17MW

AESs can thus be equipped with an ac or dc SPS. Traditionally, ac-SPSs were often preferred because of the prevalent land-based ac infrastructure, well-established power transformer, and need for ac propulsion motors [23], [24]. These ac systems use on-board generators that are connected via a CB to the ac bus, powering the shipboard loads. However, recent developments in PE devices have significantly increased the feasibility of dc grid on ships, establishing dc-SPSs as the primary research focus for future ship electrification [25]. A dc-SPS provides significant advantages in efficiency, power density, source synchronization, and ESS integration [13], [26], [27], [28], [29]. Further advantages of dc-SPSs can be

identified for naval applications. These include reduced EMI and EMC concerns, improved acoustic performance, and simplified integration of future HEW like ship-borne lasers or rail guns [30].

However, implementing dc power systems on ships presents several challenges. First, as dc system technology has yet to mature, off-the-shelf converters and protection devices for medium voltage and high power shipboard applications are limited to not available. Furthermore, the low-voltage off-the-shelf PE devices come with significant compromises on power density, efficiency, power/voltage scalability, and cost [31]. Second, maintaining the dc-grid voltage stability is challenging, especially with the presence of pulsed loads [11], [32]. This issue arises because the bus-connected PE converters operate as constant power loads under rapid terminal voltage/current variations. Hence, these converters are seen as negative incremental impedances in the dc grid, affecting the voltage stability under rapid changes in the power demand [33]. The generator rotor angle and frequency instability issues of ac grids do not arise in dc-SPSs, as the interfacing PE converters effectively decouple the generator frequencies from the dc bus. [34].

Third, designing an appropriate Fault Protection System (FPS) for a dc-SPS posses a challenge. In contrast to ac, dc grids lack natural zero current crossings, making the well-established ac CB technology ineffective for dc application [35]. Moreover, upon a short circuit fault, the energy stored in the converters' passive filtering components is quickly released, driving the fault current. This rapid rise in current is then solely limited by the small ohmic resistance of the dc cables [36]. In contrasts, ac-SPSs have higher cable impedances that limits the fault current rise, thereby relaxing the breaking requirements of ac protection devices [22]. As a result, dc grids require a more advanced fault protection approach. Breaker-based protection of dc-SPSs relies on high-speed fuses, as well as solid-state, mechanical, and hybrid CB. Following [31], the response time of the mechanical and hybrid CB is high for shipboard application. Conversely, solid-state CB are associated with high losses. Breaker-less protection methods, that use PE converters for fault limiting and interruption, is becoming a promising alternative [37]. Further challenges involved with SPS protection arise with fault selectivity, sensitivity and implementing the grounding system [32].

Finally, ensuring the reliability of a dc-SPS is a challenging task. With the high penetration of PE devices in dc grids and the enhanced level of network interconnectivity, the system-level reliability can be significantly compromised. This especially as the fundamental components of the PE converter, the electrolytic capacitor and semiconductor devices, are among the most vulnerable parts of the system [38]. Moreover, the harsh environmental conditions of ships expose the power system components to high levels of vibration, humidity, and salinity, accelerating component degradation, thereby making the system more fragile and prone to failures [39], [40]. In addition, maintenance work on dc-SPSs is more complex than on land-based power grids. With a fixed availability of spare parts and a high dependence on operation continuity, corrective maintenance during ship operation is limited. Meanwhile, predictive maintenance of the power system is restricted to the scheduled overhaul periods. Combined, this stresses the importance of the SPS robustness and inherent ability to maintain operation under component failures, making reliability assurance a critical yet challenging part of the dc-SPS design.

As the functionality of the power system is vital to both the vessel mission and crew safety, ensuring the SPS reliability is critical for the adoption of the dc-AES [20], [37]. However, as the reliability aspect of the SPS imposes a tradeoff with other performance parameters, such as affordability, efficiency, and power density, a design must be implemented that maximizes the system's reliability at a minimal expense. This reliability-oriented design should optimize the structural arrangement of the dc grid and improve the incorporation of PE devices and protection equipment to benefit the load supply adequacy. While other reviews like [25], [31], [32], [33] have addressed many aspects of the shipboard dc-bus and power-system design, no discussion was provided on how these design parameters impact vessel's reliability performance, especially in tradeoff to other performance parameters. From the field of reliability, [38], [41], [42], [43] provide overviews on PE-based system reliability modeling, yet they lack the connection to the shipboard application. To address this gap, this article provides a comprehensive overview of the reliability aspect of dc-SPSs, considering the impact of the power system design, addressing the methods used to perform adequacy assessment, and discussing strategies to improve reliability. The key contributions of this article are as follows.

1) Provide an overview of the guidelines, standards, and common practices in the design of dc-SPSs, thereby revealing the tradeoffs between reliability and other performance parameters in the dc-bus design and power system topology selection in Section II.
2) Develop a hierarchical reliability model framework for the adequacy assessment of dc-SPSs, thereby providing insights into the component-level and device-level reliability modeling, as well as comparing multiple system-level methods in Section III.
3) Provide an overview of the different dc-SPS reliability enhancement methods, addressing strategies at the component, device, and system level in Section IV.

Finally, Section V concludes this article.

II. SHIPBOARD POWER SYSTEM DESIGN

The SPS or IPS of an AES serves as the interconnecting grid among the distributed power modules. The system is designed to enable the power flow from the generation modules and ESS to all electrical loads in the vessel. While, in a traditional ship, the electric power system and propulsion power system operate as two separate circuits, the SPS supplies power to all vessel loads, regardless of their size and function. An overview of the power modules in dc AESs, with their

TABLE 2. Overview of the dc-SPS's Power Modules, With Their Common Implementations and Main Vendors

PGM:		PLM:		PCM:		ESS:	
Examples:	Vendors:	Examples:	Vendors:	Examples:	Vendors:	Examples:	Vendors:
1. Diesel generator	ABC	1. Shaft motor	ABB	1. Diode bridge rectifier	ABB	1. Intergated battery	Corvus
2. Gas turbine generator	Hyundai HI	2. Thruster	GE Vernova	2. Active bridge rectifier	Danfoss	2. Containerized battery	EST-Floattech
3. Fuel cell	MAN	3. Radar and navigation	Indar	3. Two-level inverter	NES	3. Super capacitor	Leclanché
4. PV system	Nedstack	4. Lighting	Kongsberg	4. Multilevel inverter	Schneider E.	4. Flywheel	Saft
5. Nuclear reactor	RR / MTU	5. Heating and cooling	Siemens	5. DC–DC converter	Siemens	5. Compressed air	Shift
6. Methanol engine	Wärtsilä	6. Auxiliary loads	WEG		The Switch		Siemens

Vendors are ordered alphabetically.

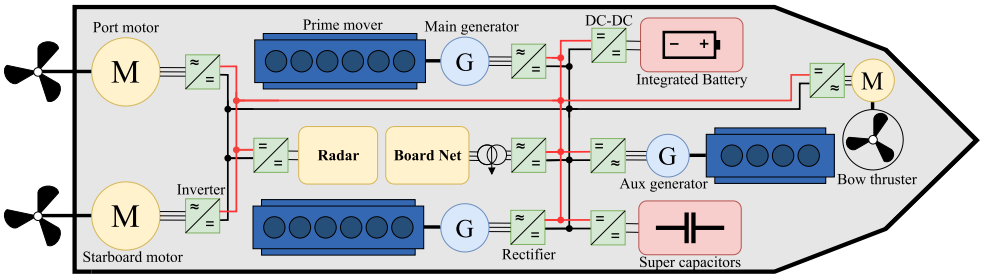

FIGURE 1. Notional AES with a simplified dc-SPS.

common implementations and main vendors, is provided in Table 2 [25], [44], [45]. Moreover, a notional AES with a simplified dc-SPS model is provided in Fig. 1.

With most of the world's fleet relying on diesel engines for power generation and propulsion, diesel generators are the most common PGM implementation to energize a SPS [46]. Alternatively, less common prime movers, such as gas turbines, LNG engines, and nuclear reactors, can be used to power the system. However, with recent innovations in methanol engines and hydrogen fuel cells, promising sustainable energy supply alternatives are entering the market [47], [48]. Although the majority of vessels still use conventional fuels (HFO, MDO, MGO), the adoption of alternative fuels is rapidly rising [46]. As of June 2024, over 27% of the ships on order utilize alternative fuels, representing about 50% of the order gross tonnage [46]. In addition, large advancements are being made in utilizing ammonia as a maritime fuel. The zero-carbon emissions of green ammonia makes the carrier a promising alternative to carbon-based fuels. Meanwhile, the energy density of ammonia is higher than clean alternatives, such as hydrogen and Li-ion batteries, making storage simpler and more affordable [49]. As a result, manufacturers including MAN, WinGD, and J-Eng are developing two-stroke ammonia engines while Wärtsilä and Hyundai HI are developing four-stokes. Although currently no large dc vessels are powered using ammonia, demonstrators have shown their functionality. In 2024, the *Sakigake* tugboat became the first commercial vessel to use an ammonia-fueled engine. Later that year, the *NH3 Kraken* used a full-cell-based ammonia powerpack from Amogy to power its 750 kW propulsion motor and electrical system.

After generation, power is applied to the dc-bus using the PCM. Besides voltage transformation, these modules provide power flow control and can embed protection functionalities, like fault current limiting and galvanic isolation [31]. The output power of the PCM is then distributed throughout the vessel using a dc-bus. Although absent in the simplified power system of Fig. 1, the dc-bus contains various protection devices, such as CB, disconnectors, and high-speed fuses, fragmenting the dc-bus in zones to improve the resilience of the power system. Multiple vendors including ABB (*SACE Infinitus*), AstrolKWx (*Marine dc-Breaker*), and The Switch (*EDCB*) provide solid-state circuit-breaking solutions for LVDC maritime applications. Finally, the power is supplied to PLM via another set of PCMs. The load profile of an AES is typically dominated by the vessel's propulsion load. Service loads, such as the radar, lighting, and heating/cooling system, vary dynamically throughout the day, though small in comparison to the propulsion load [45].

A. DC-SPS GUIDELINES

For the design of a dc-SPS, limited guidelines and standards have been provided in literature. *IEEE Std 1709-2018* provides standards and recommendations for MVDC power systems on ships [34]. It considers a notional MVDC SPS and provides general requirements on voltage ratings, grounding, isolation, stability, and protection. *IEEE Std 45.1-2023* focuses on the design of electrical installations on ships and provides recommended practices addressing ac and low-voltage dc power systems [50]. *IEC 60092-201* provides general requirements for ship power system design with a minor focus on dc distribution, and *IEC 60092-202* offers general standards for the protection of SPSs [51], [52]. Finally, *IEC 63108-2017* defines some aspects of primary dc distribution on ships [53]. Peyghami et al. [41] aim to bring together the different aspects of dc-SPSs, by providing an overview of the transient and steady-state design specifications and requirements. Finally, the electric ship research and

TABLE 3. Overview of the SPS Recommended Voltage Classes Based on *IEEE Std 1709-2018*, *IEC 60092-201* for dc and *IEEE Std 45.1-2023* for ac [34], [50], [51]

DC class: V_{dc}			AC class: V_{ac}
	Unipolar	Bipolar	Utilization / Generation
LVDC	750 V		440 / 450 V
	1 kV		460 / 480 V
MVDC	1.5 kV	±0.75 kV	575 / 600 V
	3 kV	±1.5 kV	660 / 690 V
	6 kV	±3 kV	3.3 / 3.3 kV
	12 kV	±6 kV	4.16 / 4.16 kV
	18 kV	±9 kV	6.6 / 6.6 kV
	24 kV	±12 kV	11 / 11 kV
	30 kV	±15 kV	13.8 / 13.8 kV

The ac voltages are three-phase line-to-line and rms.

development consortium has provided two notional MVDC SPS at 5 kV and 12 kV in [54] and [55], respectively.

B. DC-BUS DESIGN

The dc bus is an integral part of a dc-SPS. Its design provides considerable flexibility in selecting the voltage level, bus configuration, and grounding topology (Earthing). However, each option comes with its merits and demerits, impacting the operating performance and long-term reliability of the SPS.

1) VOLTAGE LEVEL SELECTION

A critical and intricate element in the design of a dc-SPS is the bus voltage selection. According to the standards in [34], MVDC SESs are recommended to operate at one of seven voltage classes, as listed in Table 3. This table also includes the two highest LVDC voltage classes proposed in [51] and the ac three-phase line-to-line voltage classes defined in [50]. The selection of a SPS's dc-bus voltage typically depends on the vessel power rating. Following [29], an LVDC system can feasibly power a vessel with a total load of 20 MW. Meanwhile, MVDC systems can be utilized for ships with power ratings up to and above 100 MW. Hence, the decision between LVDC and MVDC is primarily based on the vessel's power requirements, which is typically dominated by the propulsion load.

Selecting a power system's optimal MVDC voltage is further determined by the desired generator voltage, propulsion motor voltage, load considerations, standard cable ratings, and the arc fault energy [34]. Selecting a high dc-bus voltage reduces the system's conduction losses, generally benefiting the efficiency, power density, or power transfer capacity of the SPS [56], [57], [58]. However, a higher bus voltage comes with the downside of increased isolation and safety requirements [34]. Moreover, it raises the blocking voltage and voltage gain requirements of the PCMs, imposing the need for more complex converter topologies, such as MMC-based inverters, rectifiers, and dc–dc converters [44]. Although MMCs provide enhanced power/voltage scalability, efficiency, reliability, fault protection, and reduced motor/generator insulation

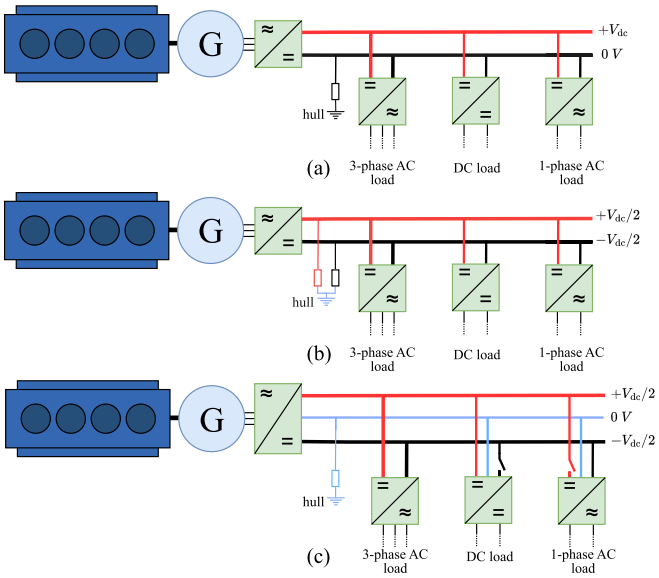

FIGURE 2. Simplified shipboard dc bus in (a) unipolar configuration, (b) bipolar without distributed neutral, and (c) bipolar configuration with distributed neutral.

requirements, it does come with a higher design complexity and cost as well as a reduced power density [29], [56], [59], [60], [61]. Selecting a low dc-bus voltage offers the advantages of simplicity and COTS availability, though it also imposes increased distribution losses and reduced scalability. This, as enhancing the system's power capacity, is mainly achieved through the parallel configuration of PCMs [31]. Therefore, selecting the optimal dc-bus voltage is an optimization problem that heavily depends on the vessel application and performance requirements.

2) UNIPOLAR AND BIPOLAR

Besides the voltage level selection, a shipboard dc bus can be designed in a unipolar or bipolar configuration [62], [63], [64]. A unipolar dc-bus transfers power through two conductors (+ and − pole) from which one must connect (with a high impedance) to the ship's hull functioning as ground [65], [66]. The shipboard loads and generators are then connected to the bus via a PCM, perceiving the full dc potential V_{dc}, as shown in Fig. 2(a). In contrast, a bipolar dc system consists of three terminals: a + pole with a positive potential, a − pole with a negative potential, and a neutral at zero potential. Similar to a unipolar system, a bipolar dc bus can transfer power using two conductors (without distributed neutral), as shown in Fig. 2(b) [34]. The parallel impedance grounding then forces the neutral potential close to ground, imposing a $+V_{dc}/2$ and $-V_{dc}/2$ at the two poles [66]. Alternatively, a tree-conductor bipolar dc bus can be selected where the neutral is distributed with the two poles, as shown in Fig. 2(c) [62], [65], [66]. In this configuration, the generator powers the system through a three-level inverter, which may be implemented using a three-L neutral point clamped converter or two cascaded 2L

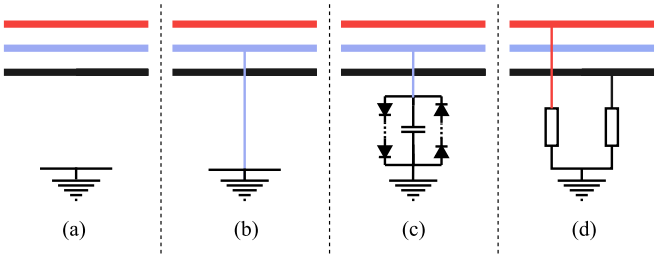

FIGURE 3. Common grounding strategies bipolar dc bus (a) ungrounded, (b) solid, (c) TN-SCD, and (d) high resistance.

converters [67]. With the tree-conductor system, high power loads are connected pole-to-pole, perceiving the full dc-bus potential. Meanwhile, low power loads are connected pole-to-neutral and thus perceive $V_{dc}/2$.

A bipolar dc-SPS with distributed neutral can provide a higher power density, design flexibility, and reduced isolation requirements when compared to a unipolar system [25], [62]. Moreover, the system provides improved reliability and survivability aspects, as it contains inherent redundancy for critical load modules. With reconfiguration, these modules can be fed from either the + or − pole, making them fault tolerant against single pole-to-neutral faults. However, maintaining system stability in a bipolar dc-SPS is challenging due to the possibility of power flow imbalances between the poles. This issue imposes the need for a voltage-balancing circuit and a more complex control strategy. [31], [62], [68].

3) GROUNDING AND CORROSION

Selecting a proper dc-bus grounding scheme is critical for staff safety and the prevention of vessel corrosion. Since direct currents cause severely more rusting than alternating once, an inappropriately Earthed dc-SPS can lead to long-term structural hull damage [62], [65], [69]. Corrosion due to dc stay currents is widely studied for transit systems [70]. In these systems, the finite conductance of the rails causes some current, known as stray current, to flow outside the intended return path, instead using nearby pipes and steel structures as conductors. At the points where these stray currents exit the metal structure, an anodic reaction causes corrosion, damaging the infrastructure. [71]. A similar reaction may occur in dc-SPS applications, where the ship's hull interfaces with the seawater. A proposed (but not recommended) grounding scheme in [34] is a monopolar dc bus, where the ship's metal hull functions as the return conductor. Like the rails, the finite conductance of the hull causes a stray current to flow through the seawater, imposing (accelerated) hull corrosion. Using the hull as a current path is therefore highly discouraged [34].

Fig. 3 provides four common topologies for grounding a bipolar dc bus. The ungrounded strategy, shown in Fig. 3(a), offers the advantage of a simple grounding system implementation, a low pole-to-ground fault current, as well as a negligible stray current corrosion [34], [72]. However, protecting an ungrounded dc system is challenging, leading to safety issues when considering MVDC [73]. A solidly grounded dc bus, as shown in Fig. 3(b), offers the advantage of a low common-mode voltage and simple protection system integration, benefiting the bus's safety aspects for MVDC [72]. However, given that the neural wire is solidly grounded at multiple locations, any voltage drop across that conductor (caused by power imbalances) imposes a hull current, resulting in stray current corrosion [74]. To solve this issue, TN-SCD grounding, as shown in Fig. 3(c), is proposed. This strategy uses the diode forward voltage to counteract a voltage drop across the neutral wire but keeps the near-ground potential under fault conditions [74], [75]. While both solid and TN-SCD grounding provide safety benefits, they encounter a large current under pole-to-ground fault conditions. As in maritime applications, dc power systems are expected to be single pole-to-ground fault-tolerant, high resistance grounding is often preferred. This grounding topology, shown in Fig. 3(d), perceives minor stray currents due to the large grounding resistors in series with the hull path. Moreover, upon a pole-to-ground fault the system can maintain temporal functionality with a $V_{dc}/2$ voltage shift on all three conductors [71].

Although stray currents are minimized with high resistance grounding, a bipolar configuration offers further benefits over a unipolar topology. In a multigrounded bipolar dc bus, the voltage drop across the neutral conductor is zero under balanced load conditions, eliminating steady-state currents through the hull. In contrast, the return line of a multigrounded unipolar dc bus experiences a small voltage drop, potentially resulting in a minor steady-state stray current.

C. POWER SYSTEM DESIGN

In addition to the dc-bus configuration, the SPS design offers flexibility in selecting the network topology. This topology refers to the structure used to interconnect the distributed modules of a dc-SPS. Although several network designs have been proposed in the literature, dc-SPSs can be categorized into five main types: the radial topology, ring topology, zonal topology, hybrid ac–dc topology, and BAAH topology. Fig. 4 provides examples of these five topologies for a simplified dc-SPS. These power systems are designed with two shaft propulsion motors (port and starboard), four generators (two main and two auxiliary), two ESS, and multiple load centers.

The primary function of a dc-SPS is to securely interconnect the distributed power modules under all operating conditions. However, these maritime power systems face highly dynamic load profiles and harsh environmental conditions, making module breakdowns inevitable over the vessel's lifetime [39], [76]. Nevertheless, the ability of the SPS to manage these intrinsic faults depends strongly on the network topology [77]. Besides the impact on reliability, the power system topology affects other performance parameters, including the power density, simplicity, efficiency, affordability, and survivability. Consequently, the topology selection possesses a tradeoff between the reliability and other system performance parameters. To secure an optimal topology for a

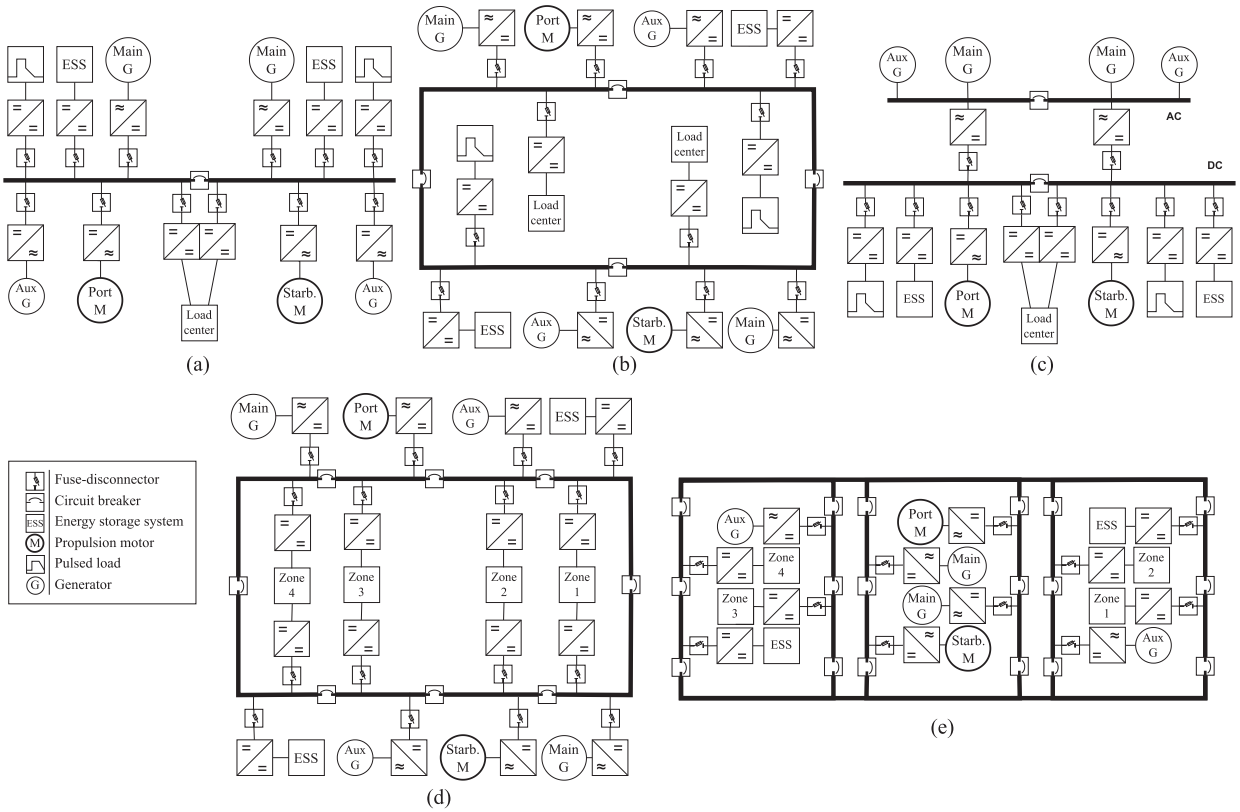

FIGURE 4. Simplified DC-SPS in the (a) radial topology, (b) ring topology, (c) hybrid ac–dc topology, (d) zonal topology, and (e) BAAH topology.

specific vessel application, it is essential to to analyze how the performance metrics vary across the topologies. Therefore, the rest of this section provides an overview of the five main SPS topologies, introducing their designs and comparing their performance aspects.

1) RADIAL TOPOLOGY

The radial SPS topology, provided in Fig. 4(a), is introduced as a conventional architecture in *IEEE Std 1709-2018* for dc and in *IEEE Std 45.1-2023* for ac applications [34], [50]. This topology is based on a common MVDC bus that directly interconnects all shipboard loads, storage devices, and generation modules. As proposed in [34], all modules must be connected to the dc bus via a fault current limiting PE converter and a disconnect switch. Combined, these devices function as the protection system, minimizing the need for load-side CB. On top of that, it is recommended to protect ac-powered substations from faults using ac CB. Further system protection is achieved through the placement of a bus-tie dc CB between the port and starboard sides of the bus, allowing the two sides to operate independently in the event of a fault.

In [45], several ac applications of the radial power system are presented, including a 690 V/60 Hz passenger ferry, a 11 kV/60 Hz cruise ship with a 440 V service load, and a 6.6 kV/60 Hz LNG tanker using a 24-pulse diode rectifier and voltage source inverter to excite the asynchronous motors. In addition, a naval frigate is discussed that uses a 6.6 kV radial topology to power two propulsion motors in a hybrid configuration with two gas turbines. Shekhar et al. [78] explored the merits of a radial dc-SPS as compared to the ac alternative. It highlights the gain in efficiency, safety, and reliability that can be achieved at different segments of the dc power system. A further comparison between radial ac and dc is made in [24], which analyses the efficiency and fuel consumption of a conventional diesel–electric cruise ship. Without incorporating a battery ESS, the complete power system had an energy efficiency of 37.0% in the ac configuration and 39.0% in dc. This energy efficiency was later improved to 42.4% and 42.9% for ac and dc, respectively, when using batteries as spinning reserve. In [79], the weight benefits of the radial dc power system are discussed. For a platform supply vessel, the weight of the SPS was reduced from 116 to 85 t when changing from an ac to a dc grid. In [80], the radial power system topology is applied to a naval vessel, posing the first step of integrating variable frequency ac (VFAC). The authors showed a theoretical average reduction in fuel consumption of 5% for an auxiliary tanker with VFAC, while highlighting the further potential of a dc system to be smaller, lighter, and more efficient. Overall, the radial topology is widely represented in literature for studying both ac and dc configurations.

2) RING TOPOLOGY

While the radial topology was constructed with two dc-bus segments, large ships often require further power system

segregation to ensure system resilience. The ring topology, provided in Fig. 4(b), has a port and starboard side dc bus, which connect at the bow and stern of the vessel using dc-CBs. To further improve resilience, dc breakers separate the two busses with a fore-aft split. With closed breakers, this topology creates a ring-like power system connecting all shipboard loads, storage devices, and generation modules, via a PE converter and a disconnect switch [34]. While a closed CB configuration is not a necessity for the functionality of the ring topology, it does provide substantial fuel and emission savings [81].

In [82], a ring-based SPS is implemented for an LNG tanker. Its 6.6 kV/60 Hz power system connects two 11 MW propulsion motors to four diesel generators. The authors also propose two dc alternatives, including a dc–ac hybrid and a full MVDC ring power system. The ring topology is also applied for naval vessels in [83] and [84], where the latter SPS has four main and two emergency switchboards forming a ring-like power system structure. In [85], a ring-structured SPS is implemented for a semi-submersible drilling rig. This 11 kV/60 Hz ring distribution network transfers power from eight 5.2 MW generators to eight 3.2 MW positioning thrusters and the 690 V board net. As a drilling rig is a dynamic positioning vessel, the propulsion system is required to be fault tolerant against first-order failures, ensuring an uninterrupted station keeping of the ship [86]. For this reason, the power system requires four switchboards, each connecting to two generators and two azimuth thrusters. Upon a segment fault, the four-split power system can isolate the faulty segment by switching off the nearest CB, establishing uninterrupted station keeping via the three remaining segments. This ability to operate a critical load with a single-point failure provides a significant reliability and survivability advantage over the two-split radial structure. Moreover, the enhanced interconnectivity of the ring topology imposes two alternative paths for power transfer, which improves load-shedding performance upon module faults. However, the alternative transfer paths do impose a protection challenge. Depending on the location of a fault, high currents can flow in either direction and be supplied from multiple sources, thus requiring a more sophisticated protection strategy. Overall, the increased interconnectivity and segmentation of the ring topology can improve reliability and survivability at the expense of simplicity and cost.

In [87], a comparative fault study is conducted for the radial and ring topologies to analyze the impact of these architectures on the SPS resilience. For the two topologies implemented with equal generation capacities, a three-phase fault was simulated on the LV bus. Under this fault condition, the MV side voltage drop of the radial and ring topology was found to be 22% and 14%, respectively. This indicates a more survivable character of the latter topology. However, due to the ring topology's reduced path impedance and parallelism, the short circuit current was simulated to be 24% higher than in the radial alternative. A qualitative comparison of the two topologies is performed in [25], where the Xu et al. [25] mentioned that the ring topology offers superior reliability, survivability, and reconfigurability at the expense of an increased complexity and investment cost.

3) HYBRID AC–DC TOPOLOGY

Until now, the considered topologies used dc to distribute power, while ac modules were interfaced using individual PE converters. Although, as MVDC devices are scarce and dc system protection is challenging, the hybrid ac–dc topology is seen as a more feasible solution for the transition towards full dc SPSs [28], [82], [88]. Hybrid systems can leverage the advantages of both ac and dc distribution systems, such as utilizing the mature ac protection hardware while eliminating bulky propulsion system transformers through dc–ac inverters [82], [89]. The hybrid topology, provided in Fig. 4(c), has a port and starboard side dc bus connecting the shipboard loads and storage modules. In extension, the system has an ac bus connecting to the generators and possibly ac loads [82]. The ac and dc buses are then interconnected using a set of PE converters. In line with [28], the hybrid topology can either be configured with a primary dc bus and an ac subbus or a primary ac bus and a dc subbus.

In [82], a hybrid SPS is implemented for an LNG tanker. The proposed power system has an 11 kV ac primary bus that connects via four passive rectifiers to a 10 kV dc subbus, which powers the two propulsion motors. The authors highlight that the hybrid topology offers the advantage of requiring less invasive ship architecture modifications when transitioning from a full ac-SPS. In [87], a comparative fault study is performed for the hybrid topology with respect to the radial and ring alternatives. For the three topologies implemented with the same generation capacity, a three-phase fault was simulated in the LV bus. The MV side voltage drop on the hybrid topology was 11%, which was significantly lower than the 22%, and 14% drop of the radial and ring topologies. Moreover, it was found that the short circuit current was over 60% smaller than in both the ring and radial SPS, highlighting the protection advantage of ac. Alternative implementations of the hybrid topology can be found in [80] and [90], which discuss a high frequency and parallel ac–dc implementation, respectively.

4) ZONAL TOPOLOGY

To ensure an uninterrupted power supply of critical loads in a ring SPS, they can be connected to more than one dc switchboard [63]. However, with an increasing number of vital loads, the number of longitudinal cables would increase significantly, making the ring topology a bulky solution [22]. The zonal topology, provided in Fig. 4(d), is similar to the ring power system in that it has a port side and starboard side dc bus, connected via CBs at the bow and stern of the ship. However, in a zonal SPS, the loads are grouped into zones, which can also accommodate storage devices and generation modules. Each zone then connects via a PCM and transverse feeder cable to both the port and starboard side

dc bus. As a result of its architecture, the zonal SPS has an outstanding fault tolerance performance. When a dc-bus fault occurs, the FPS can reduce the short circuit current and isolate the faulty segment, while the critical zones can draw power from the opposite healthy bus [63]. Moreover, under multiple simultaneous system faults, the zonal SPS can perform segmentation, reconfiguration, and self-healing to improve its supply continuity [63]. So, the zonal topology improves the operational capability of an AES even under extreme operating conditions [34].

Besides the weight reduction for critical load supply, the zonal topology provides flexibility in equipment integration. Upgrading components or adding redundancy can be performed easily through the system's modular design, achieving increased reliability and survivability at a lower cost [22]. In the "next generation IPS technology development roadmap," zonal SPSs are proposed as the future topology standard to cost-effectively meet requirements on power quality, reliability, and survivability [30].

Petry and Rumburg [91] provided a cost and weight comparison of a ring and zonal SPS for a US Navy destroyer. It was found that the power system weight can be reduced from 141 t to 104 t when employing zonal over radial. On top of that, the zonal topology reduced the material and labor costs by $1.67 M per ship. A similar analysis is performed in [92], which compares the performance of an ac zonal and dc zonal configuration for a notional surface combatant. It is found that the weight and cost of the IPS can be reduced by 30.7 t and $2.39 M when choosing a dc zonal over ac. A qualitative comparison of the zonal SPS in relation to radial and ring topology is performed in [25]. The authors mention that the zonal topology performs better on reliability, survivability, and reconfigurability at the expense of complexity and cost.

5) BAAH TOPOLOGY

The BAAH topology is commonly proposed for utility power systems to enhance resilience and obtain interruption-free maintenance. Fig. 4(e) shows an example of a dc-SPS based on the BAAH topology. This system is constructed with two longitudinal busbars on the port and starboard side of the vessel, interconnected through a series of bays. Each bay consists of two outside breakers and a common breaker in the center. All shipboard PLMs, PGMs, and ESSs are located in a bay, connected between an outside breaker and the common breaker [77]. As a result, each module is protected by a "BAAH," which ensures functionality in the event of a first-order fault [93]. Effectively, the BAAH topology uses redundancy to achieve high levels of reliability and survivability.

Stevens and Santoso [77] used Markov modeling to compare the reliability of a SPS based on the zonal and BAAH topology. It is found that employing a BAAH topology over zonal reduces the failure rate of the pulsed load and ESS by 17% at the expense of the radar and propulsion system reliability. Meanwhile, following [20], the overall service interruption rate of the SPS is reduced from 0.27 #/y with zonal to 0.22 #/y with the BAAH topology. An essential aspect of the BAAH topology is that a module's placement is of great significance to its reliability. Loads paired with a PGM, like the starboard motor in Fig. 4(e), maintain operation even when both busbars fail. The optimization of module placement in a BAAH SPS is discussed in [20], where the Stevens et al. [20] proposed a module location optimization algorithm that maximizes system reliability, demonstrating superior reliability performance after relocation. Another reliability improvement for the BAAH topology is proposed in [93], which suggests the usage of sectionized busbars by adding CBs. However, the authors found only a minor impact, lowering the load center failure rate by less than 3%. The fault tolerance of the BAAH topology is studied in [35] and [94]. In [35], the size, weight, and survivability aspects of the zonal and BAAH topology are compared, illustrating how the SPS architecture can influence the vessel's resilience. The survivability of a notional navy destroyer with a zonal and BAAH SPS is analyzed in [94]. Using a stochastic vulnerability assessment to represent a hostile environment, it was found that BAAH topology performed 1.2% worse on single-hit survivability and 5.2% worse on double-hit survivability.

An overview of the relevant studies comparing the aspects of SPS topologies is provided in Table 4. This table shows the considered voltage configuration (ac, dc, or both), the application, and the relevant power system topologies. This table aims to highlight the research focus regarding SPS topology comparisons and show the main application directions. Besides, the table might reveal some of the limitations and knowledge gaps in SPS architecture research.

D. POWER SYSTEM COMPARISON

Based on the overview of the five dc-SPS topologies, their key performance parameters can be compared. The result of this qualitative comparison is presented in the radar chart of Fig. 5, which ranks the performance of the five topologies on affordability, efficiency, reliability, survivability, power density, and integration simplicity. It can be concluded from Fig. 5 that the BAAH topology offers the highest reliability performance, followed by the zonal, ring, and radial topology [77], [25]. Although similarly structured, the hybrid topology provides a slight reliability advantage over the radial topology [101], [102]. Fig. 5 further shows that the zonal topology outperforms the BAAH on survivability [94], [100]. This performance order is then followed by the hybrid, ring, and radial topology [25], [87]. Following [103], the integration simplicity of a SPS depends on the number of PCMs, as well as the intricacy of the protection system and power/energy management strategy. Therefore, as in Fig. 5, the radial topology provides the simplest integration, followed by the hybrid, ring, BAAH, and zonal topology [25], [45].

The efficiency of the SPS also depends on the selected architecture. From Fig. 5, it is concluded that the hybrid topology has a lower operating efficiency than the full dc

TABLE 4. Studies on SPS comparisons ac, dc, and hybrid ac-dc.

Publications on SPS topologies								
Voltage:	**Application:**	**Power system topology:**					**Focus:**	**Ref:**
		Radial	Ring	Hybrid	Zonal	BAAH		
AC	Passenger, Commercial, Naval vessels	•					Introduction of different vessel applications and implementations with radial MVAC SPSs.	[45]
	Naval ship		•		•		Perspective on the transition from radial ac to zonal ac with the integration of mission systems.	[84]
	Naval ship	•			•		Weighs comparison of the radial and zonal topology on a naval vessel and analysis of the conversion cost for the DD-51 and an amphibious ship.	[91]
	General vessel	•			•		Advantages and challenges of ac zonal shipboard power systems.	[95]
AC & DC	Naval ship				•		Comparison of acquisition cost, annual fuel cost, installation cost, and size of a mechanical drive and a zonal power system ship.	[96]
	General vessel	•		•			Comparison of different configurations of radial ac to hybrid ac-dc.	[28]
	General vessel	•					Reliability comparison of a radial ac and dc shipboard power system.	[78]
	General vessel	•			•		Evolution from radial ac to zonal dc with perspectives on control and fault reconfiguration.	[63]
	Naval ship	•	•	•			Survivability and fault tolerance comparison of multiple SPS topologies.	[87]
	Cruise ship	•					Efficiency comparison of an ac and dc diesel-electric power system of a cruise ship.	[24]
	LNG tanker		•				Benefits and challenges of hybrid and full MVDC distribution for an LNG tanker.	[82]
	Naval ship	•	•	•			Advantages and challenges of MVDC over MVAC and VFAC.	[30]
	Naval ship				•		Comparison of ac and dc zonal, by cost, weight and efficiency.	[92]
	Naval ship	•			•		Comparison of radial ac to zonal ac with the further advantages to zonal DC.	[97]
	General vessel	•		•			Improving fault tolerance of a dc radial IPS by adding MVAC.	[90]
	General vessel	•		•			Comparison of MVDC radial with hybrid topology.	[88]
	Naval ship	•		•			Overview of the different dc radial topologies for future naval applications.	[80]
	Dredging vessel	•					Comparing radial ac and dc in terms of power loss for a dredging application.	[98]
DC	General vessel	•	•		•		Overview and comparison of the performance parameters of three SPS topologies.	[25]
	Naval ship				•	•	Trade-off study on weight, volume, single and double hit survivability.	[94]
	Naval ship		•		•	•	Survivability, size, and weight comparison of the topologies using breaker-based and breaker-less protection.	[35]
	Supply vessel	•			•		Perspective on the efficiency of a centralized and distributed dc power system.	[79]
	Research vessel	•					Comparison of cost, space, and mass of a radial dc SPS to radial SPS.	[99]
	General vessel				•	•	Reliability comparison of multiple dc SPS architectures.	[77]
	General vessel				•	•	Resiliency analysis of multiple dc SPS architectures.	[100]

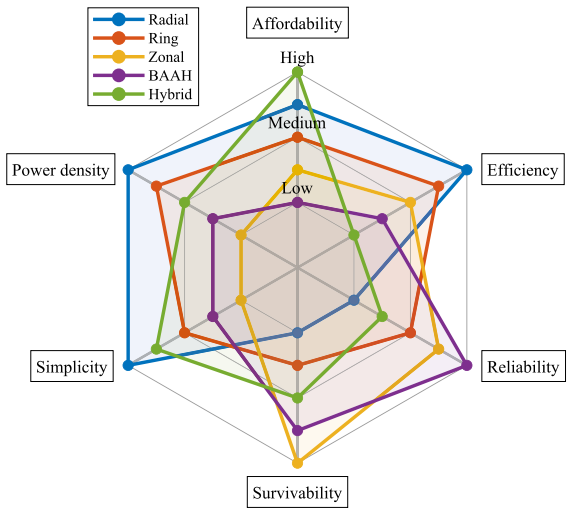

FIGURE 5. Qualitative performance comparison for the five SPS topologies.

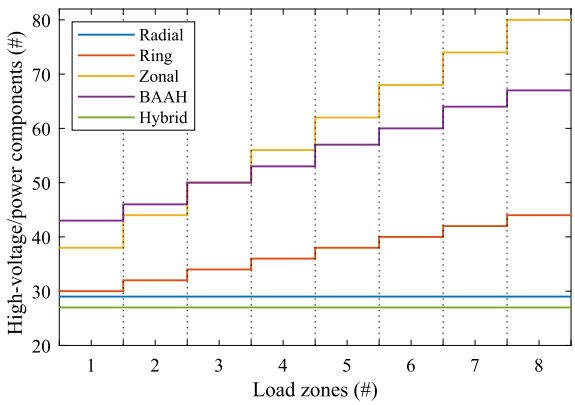

FIGURE 6. Comparison of the number of high-voltage high-power components for the five SPS topologies.

alternatives [103]. This reduced efficiency is caused by the direct connection between the diesel generators and the ac bus, imposing a fixed engine speed. Meanwhile, the full dc topologies use interfacing PCMs that allow for engine speed variations, significantly improving the generator efficiency under varying load conditions [104]. Given that the remaining four topologies have the same converter efficiencies, the CB placement imposes a difference in losses. As any power flow through a solid-state CB comes with losses, having one or multiple CBs in the power path reduces the SPS's efficiency. Therefore, given their structures, the efficiency order is defined as radial, ring, zonal, and BAAH topology.

To analyze the affordability and power density of the power system topologies, Fig. 6 can be used. This figure shows the

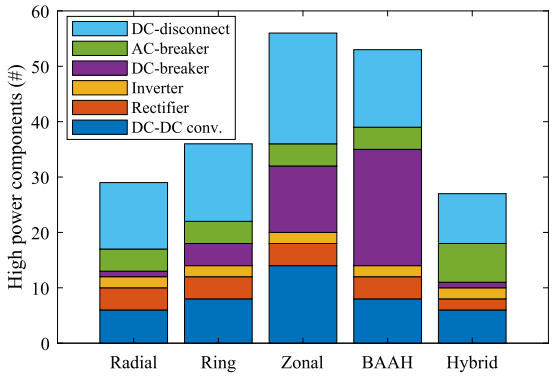

FIGURE 7. Category decomposition of the high voltage high power components for the five SPS architectures with four load zones.

total number of high voltage, high power components required for the SPS configurations in Fig. 4. The considered power systems are equipped with two shaft propulsion motors, four generators, two ESSs, and two pulsed load modules. The number of load zones in the SPS ranges from 1 to 8, allowing for an examination of the added system complexity associated with each topology.

Fig. 6 indicates that the radial and hybrid topologies demand the lowest number of SPS components. Notably, this component count remains constant regardless of the number of load zones. This is because any additional load centers are assumed to connect directly to a low-voltage dc bus, eliminating the need for extra high-voltage equipment. The zonal and BAAH topologies, due to their inherent redundancy, require the largest number of SPS components. Moreover, the zonal topology exhibits the steepest incline in component count, requiring two dc–dc converters, two dc breakers, and two disconnectors for each additional load zone.

Besides the component count, the type of components influences the affordability and power density of a SPS. Fig. 7 shows a categorized decomposition of the high voltage/power components for the five topologies when configured with four load zones. From this figure, it can be concluded that the BAAH topology is constructed using primarily dc CBs, whereas the zonal topology is fundamentally formed using the more affordable dc–dc converters. In addition, the figure shows that the radial and hybrid topologies have a comparable component count. However, the radial topology achieves protection primarily through PE converters, while the hybrid topology uses less expensive ac CB.

Following Figs. 5–7, it can be concluded that the zonal and BAAH topology excel in the reliability and survivability performance but act poorly on affordability, power density, and simplicity. The radial topology shows the opposite behavior, performing high on aspects, such as simplicity, efficiency, power density, and affordability, but at the cost of a reduced SPS resilience. Similar to the dc bus design, finding a vessel's optimal SPS topology is an optimization problem that depends on the ship's application and performance priorities. Using vessel aspects, such as the size, task, and number of critical loads, combined with the mission properties, such as the duration, location, and operating conditions, narrows down the topology selection. Performing further reliability analysis can allow for selecting the optimal SPS topology, provided the system's constraints.

III. RELIABILITY ASSESSMENT

In maritime applications, maintaining continuous load excitation is essential for both the ship's mission and its personnel safety [20]. As a result, the vessel's PGMs are consider critical components that strongly affect the performance of the AES. Research focus is therefore dedicated to the reliability assessment of generators, fuel cells, and shore charging [105], [106], [107]. However, since the SPS serves as the power transfer medium between the PGMs and shipboard loads, its reliability is equally important. Any failure in the SPS can have severe consequences on the vessel's mission and expose its personnel to an unsafe environment. Therefore, when designing a SPS, it is imperative to aim for near-zero failure rates, especially for the supply of critical loads. Effectively, the reliability of a SPS is a vital operational attribute that requires considerable attention during the design phase to ensure appropriate availability and longevity [108], [109].

The reliability R of a SPS is defined as the probability that the system functions adequately for the intended operating period under the intended operating conditions. Due to the physical nature of the power system, all components have a limited functional lifetime, where the time-to-failure exhibits a stochastic character [108]. With a nonzero probability of component failure, the SPS necessitates a robust design capable of withstanding single or multiple simultaneous failures, minimizing the frequency of service interruptions [20]. While it is possible to achieve a high SPS reliability by solely improving the component reliabilities, this comes at a significant cost. As identified by Allan and Billinton [110], reliability economics dictates that upon a fixed investment, a component encounters a decreasing increment in reliability. This suggests that as the component reliability improves, the cost of further enhancement increases, rendering a highly reliable component disproportionately expensive. Moreover, SPS components are exposed to nonideal environmental conditions including vibrations, humidity, salinity, and high ambient temperatures, which significantly increase component degradation, making module breakdowns less predictable [39], [40], [76].

While creating a highly reliable SPS is partially achieved through good component reliability, to manage the inevitable device failures, the system must incorporate enhancement techniques, such as redundancy, modularity, and reconfiguration. To optimize this investment in reliability, assessment methods are required to analyze the impact of the component adequacies and system enhancement techniques on the SPS reliability. Accordingly, the rest of this section elaborates on the SPS reliability concept, highlights the reliability indices, and provides an overview of the assessment methods.

TABLE 5. Categorization of SPS Load Point Reliability Indices, for Uninterruptible, Short-Term and Long-Term Interrupt Loads

Shipboard load point reliability indices					
Reliability index:		Unit:	Load type: Uninterruptible ①	Short-interrupt ②	Long-interrupt ③
λ	Failure rate	[#/y]	●●	●	●
μ	Repair rate	[#/h]		●	●●
MTTF	MTTF	[y]	●●	●	
MTBF	MTBF	[y]	●●	●	
MTTR	MTTR	[h]		●	●●
$R(t)$	Reliability	[]	●●	●	
$A(t)$	Availability	[]			●●
B_x	Bx-lifetime	[y]	●●	●	
D_t	Downtime per year	[h/y]			●●
π_x	Service interruption rate	[#/y]	●●	●●	●
MTBSI	MTBSI	[#/y]	●●	●●	●

A large number of • indicates a strong coherence between the load's reliability and the reliability index value.

A. RELIABILITY INDICES

To quantify the reliability of a SPS, reliability indices are used. Although, by definition, reliability is a probability measure, many other indices are commonly posed in literature. As stated in [108], the most appropriate reliability index for evaluating a system depends on the system type and goals. This index should always reflect the user's requirements and consider the intended application [38]. Accordingly, the indices used to assess SPSs deviate from the ones used to assess utility grids. The deficiency allowed with utility power grids is less to not tolerable for vital shipboard loads. This makes measures like EENS and LOLE impractical and stresses the need for a more refined set of reliability indices.

Table 5 provides an overview of the common reliability indices used to quantify load point adequacy in a SPS [50], [108], [111], [112], [113]. This table introduces the failure rate λ and repair rate μ, which are the number of failures/repairs a system encounters per unit exposure time. Using λ and μ, the MTTF, MTTR, and MTBF can be derived in accordance with [113]. The load point reliability $R(t)$, is defined as the probability that the system maintains functional throughout the operating period $[0, t]$, whereas the availability $A(t)$ is defined as the probability that the system is found in a functioning state at time t. Both $R(t)$ and $A(t)$ are given in (1). Other reliability indices like the B_x-lifetime (time at which $R(t) = x\%$) and the downtime hours per year D_t are derived from the $R(t)$ and $A(t)$ curves, receptively

$$R(t) = \mathrm{P}[t_{\mathrm{fail}} > t] \qquad A(t) = \mathrm{P}[\mathrm{State}(t) = \mathrm{up}] \tag{1}$$

While these indices can each represent the supply reliability of a load, they fail to account for the unique load characteristics and grid aspects of SPSs. Unlike the reliability analysis of utility grids, the properties of all load modules are known by the power system operator. Upon selecting a vessel operation mode, all loads have a tolerable power interruption time and a predefined load priority [114]. This imposes a more intricate reliability framework, where some loads can be shed with a lower impact on the overall performance, especially for short fault durations. Moreover, in contrast to the reliability analysis of electric aircraft, small power system repairs can be performed with the vessel in operation. This highlights the importance of component repair times, which heavily depend on the availability of spare parts.

To address these unique properties, the U.S. Navy introduced the QoS metric, which is calculated as the MTBSI [50]. As stated in [115], not all supply interruptions in a SPS lead to a system failure, as some loads, such as refrigerators or the onboard climate system, can be interrupted for several minutes without causing discomfort. Therefore, a service interruption is defined as a supply interruption that lasts longer than the load can tolerate [112]. In [50], loads are classified into three categories: uninterruptible loads, short-term interrupt loads, and long-term interrupt loads. Uninterruptible loads are modules that cannot tolerate a service interruption greater than the reconfiguration time $t_1 \in [0.1\ \mathrm{ms}, 0.2\ \mathrm{s}]$. Examples of uninterruptible loads are control computers and communication/navigation devices. Short-term interrupt loads can, due to their internal inertia or usage frequency, tolerate a service interruption with a duration greater than t_1, but will lose functionality before the generator start time $t_2 \in [1\ \mathrm{min}, 5\ \mathrm{min}]$ [112]. Examples of these short-term interrupt loads are the ship's lighting system, cooling system, and devices with backup battery power. Long-term interrupt loads, including the climate control system and galley equipment, have a high-internal inertia or low usage frequency allowing a service interruption with a duration greater than t_2. All shipboard loads are assigned a category based on the vessel configuration and its operation mode. As a result, the MTBSI of a load module accounts for both the SPS functionality and the load's inherent fault tolerance. By incorporating this mission-based load priority in the MTBSI, the metric only reflects the interruptions that compromise the vessel's mission, making it an accurate measure of the SPS reliability. Following [115], the MTBSI of a naval SPS should be in the vicinity of 3.4 years.

To better demonstrate the impact of a supply interruption on SPS performance, Fig. 8 is provided. This figure shows the

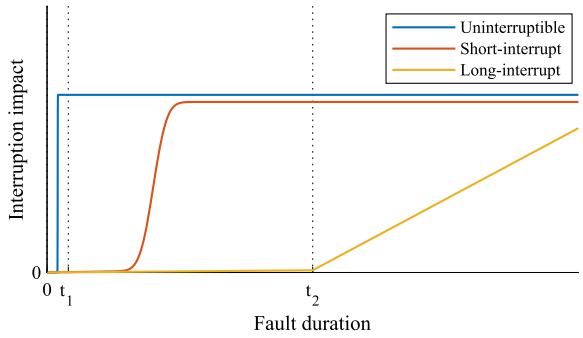

FIGURE 8. Impact of a service interruption on the SPS performance as a function of time for different load categories: Uninterruptible load, short-term and long-term interrupt loads.

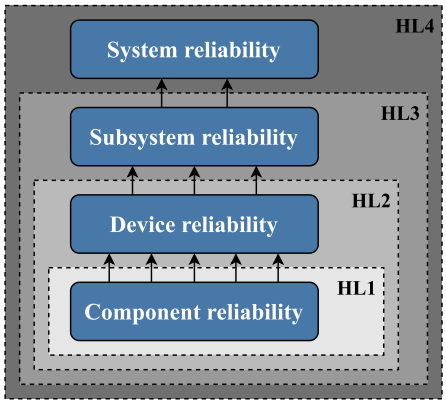

FIGURE 9. Reliability model framework for a SPS using four hierarchical levels.

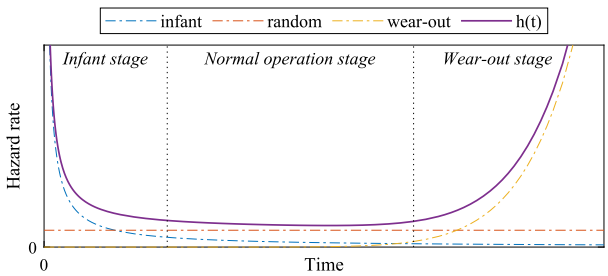

FIGURE 10. Component hazard rate curve for the infant, random, and wear-out failures, combined giving the bathtub curve.

supply interruption impact for the three load categories as a function of the fault duration. It is observed that an uninterruptible load supply failure instantly harms the power system performance. Meanwhile, the short-term and long-term interrupt loads show a delayed and more gradual performance degradation. Following this observation, the reliability indices listed in Table 5 can be ranked based on their effectiveness in reflecting a load's "true" reliability, accounting for its properties [116]. In Table 5, a large number of dots represents a high index effectiveness.

B. RELIABILITY MODEL FRAMEWORK

A quantitative reliability assessment of a SPS is critical for verifying the design specifications as well as getting insight into the impact of the power system topology, devices, and enhancement techniques on the system's adequacy [38]. However, this assessment is challenging as the SPS is a complex network interconnecting numerous components. To analyze the reliability of these PE-dominated systems, a multilevel hierarchical reliability model can be employed. This model fragments the power system into its main functional zones, creating segmentation and hierarchy in the reliability assessment [117]. Billinton and Allan [118] proposed to split a utility power system into the generation, transmission, and distribution facilities to simplify the assessment process. Similar segmented reliability frameworks are presented in [101] for electric aircraft and in [43] for PV systems.

Fig. 9 shows the reliability model framework for a SPS using four hierarchical levels. In this figure, the power system is divided into multiple subsystems, each representing a single functionality of the ship, like the propulsion system, ESS, and the board net. Each subsystem contains multiple devices, such as PGMs, PLMs, and PCMs. These devices are constructed using components like semiconductor switches, capacitors, and inductors. In Fig. 9, the HL1 analysis only considers the component reliability, incorporating the component's physical failure rates, loading conditions, and environmental stresses [101]. HL2 analysis uses the results of HL1 to determine the failure rate of a device. This HL2 assessment can include component redundancy as a way of improving the device reliability. HL3 analysis takes the device reliability to define the adequacy of a subsystem. This high-level reliability assessment incorporates the impact of device repair times and system enhancement techniques, such as redundancy, modularity, and reconfiguration. Finally, the HL4 analysis evaluates the full SPS reliability by combining the reliability indices of the vessel's subsystems. Depending on the application and operation, some subsystems are assigned a lower priority, thus contributing less to the HL4 results.

C. COMPONENT RELIABILITY

Supply interruptions in a SPS are primarily caused by faults in the system's components. These component failures can be classified into systematic failures, random change failures, and wear-out failures [119]. While systematic failures can be removed through modifications in the system's design and manufacturing process, random change and wear-out failures are inherent to the physical system. Following other engineering systems, the failure characteristics of a component can be modeled in three stages: the infant stage, normal operation stage, and wear-out stage, as shown in Fig. 10 [120]. This figure provides the hazard rate $h(t)$, the number of failures per unit exposure time, as a function of the operation time. Furthermore, Fig. 10 shows the decomposition of $h(t)$ into the three failure types. During the infant stage, systematic failures related to the debugging and manufacturing process

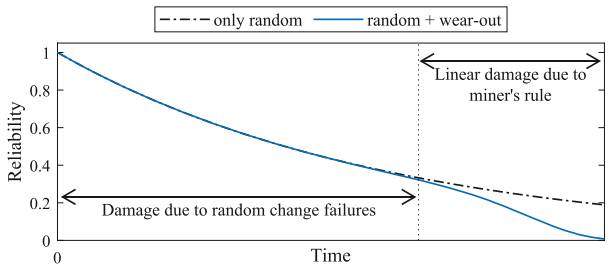

FIGURE 11. Component reliability curve using the hazard rate curves of random failures and random + wear-out failures.

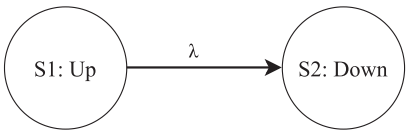

FIGURE 12. Two-state Markov model of an unrepairable component.

dominate $h(t)$ [121]. After some time, the component enters the normal operating stage, where infant failures have been mitigated, and random change failures start to dominate. These random chance failures, modeled using a low constant hazard rate λ_c, are a consequence of sudden overstress events, like component-imposed overvoltages or overcurrents [120]. Finally, during the wear-out stage of the component wear-out failures start to dominate, increasing $h(t)$. These wear-out failures are associated with the aging and internal degradation of a component, causing faults like bond wire lift-off and solder joint cracking [121], [122].

Assuming all systematic failures have been mitigated throughout the infant stage, the SPS components encounter solely random change and wear-out failures. Consequently, these components have a limited functional lifetime, where the time-to-failure exhibits a stochastic character. To model this stochastic lifetime behavior, a Weibull distribution can be used, which has a failure density function $f(t)$ and hazard rate function $h(t)$ as given in (2) [122]. In (2), α and β are the characteristic life and shape parameter of the Weibull distribution, respectively

$$f(t) = \frac{\beta t^{\beta-1}}{\alpha^{\beta}} e^{-(\frac{t}{\alpha})^{\beta}} \qquad h(t) = \frac{\beta t^{\beta-1}}{\alpha^{\beta}}. \tag{2}$$

As indicated in Fig. 10, throughout the normal operating stage, a component encounters purely random change failures with a constant hazard rate λ_c [38]. Following (2), the connected shape parameter β of the Weibull distribution must be 1, giving an exponential failure density function. The corresponding reliability curve $R(t)$ for a component that only encounters random change failures is given in (3) and plotted in Fig. 11. This unrepairable component can also be modeled as a two-state Markov model as given in Fig. 12

$$R(t) = e^{-\lambda_c t}. \tag{3}$$

To complete the reliability model, the component failure rate λ_c should be estimated. As proposed in [122], this can be done using field data, test data, stress-strength analysis, or a combination of the three. Historical failure data of identical components in identical conditions is preferred for accurate reliability modeling. However, these datasets are usually missing or come after the design phase of the power system. Therefore, industrial handbooks can be used to provide base failure rates or adapt historical failure rates to consider other operating conditions. An example of generic failure rates for various power system components is provided in *MIL-HDBK-217F* [123]. Following this handbook, the failure rate model of an IGBT can be expressed as in (4). In (4), the components base failure rate ($0.00074\,\#/10^6\,\text{h}$) is scaled using the operation dependent temperature factor π_T, application factor π_A, power rating factor π_R, voltage stress factor π_S, quality factor π_Q, and environment factor π_E, as defined in (5) till (10), respectively. Notice that the high π_E value reflects the impact of marine stressors, inducing enhanced vibrations, humidity, and salinity, on the component reliability

$$\lambda_{igbt} = 0.00074 \cdot \pi_T \pi_A \pi_R \pi_S \pi_Q \pi_E \quad [\#/10^6 \text{h}] \tag{4}$$

$$\pi_T = e^{-2114\left(\frac{1}{T_j+273} - \frac{1}{298}\right)} \tag{5}$$

$$\pi_A = 0.7 \qquad \text{Switching} \tag{6}$$

$$\pi_R = P_r^{0.37} \tag{7}$$

$$\pi_S = 0.045 e^{3.1 * \frac{V_{app}}{V_{rated}}} \tag{8}$$

$$\pi_Q = 1.0 \qquad \text{JANTX quality} \tag{9}$$

$$\pi_E = 9.0 \qquad \text{Naval applications.} \tag{10}$$

Alternatively, the *IEC-TR 62380* report provides generic component failure rate values, thereby taking into account the mission profile [124]. *FIDES* extends this constant failure rate estimation by considering the manufacturing process, operation, maintenance, and physics of failure [125]. A large advantage of *FIDES* over the other two handbook methods is its ability to incorporate the actual marine stressors, including the ship's humidity and vibrations, in the failure rate estimate.

After the useful lifetime of the component, wear-out failures start to dominate, causing a significant rise in $h(t)$. These wear-out failures can be modeled through stress-strength analysis based on a component's lifetime model and subjected mission profile [122]. This type of reliability modeling requires knowledge of the physics of failures and the potential failure mechanisms of a SPS component. The wear-out failure reliability modeling of PE components is elaborately discussed in [120], which uses the linear Miner's rule as well as lifetime models for the capacitors [38] and semiconductor devices [126]. Following [120], the component's wear-out failure rate $\lambda_w(t)$ is defined using Weibull parameters α and β. The total failure rate of a component is then modeled as the sum of the constant random change failure rate and wear-out failure rate, as given in (11). The corresponding reliability

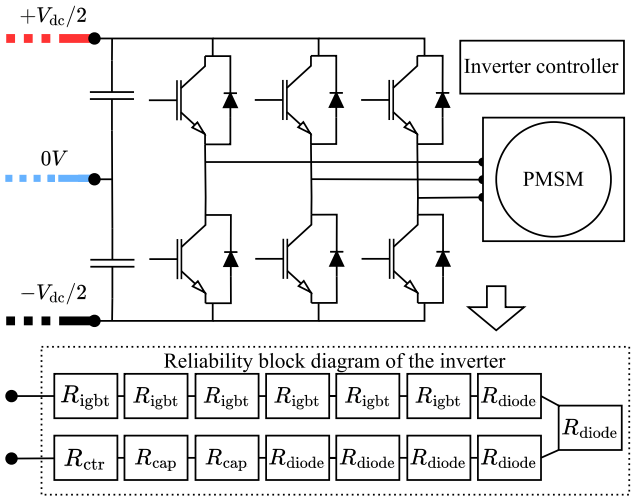

FIGURE 13. Reliability model of a two-level propulsion drive inverter.

curve is calculated using (12) and plotted in Fig. 11

$$\lambda_{cw}(t) = \lambda_c + \lambda_w(t) \tag{11}$$

$$R(t) = exp\left(-\int_o^t \lambda_{cw}(\tau)\, d\tau\right). \tag{12}$$

D. DEVICE RELIABILITY

After completing the component reliability analysis (HL1), the results are combined to assess the adequacy of a device. This HL2 analysis defines the reliability of a device as a structural combination of the component reliabilities using the functionality relation between the module and its components. For a device with no inherent redundancy, the performance relies on all of its components. Hence, a single component fault imposes a direct device failure. The reliability model of these fault-intolerant devices is considered a series structure of the component reliabilities, as provided in Fig. 13 for a two-level propulsion drive inverter [38]. For this converter, the six IGBTs, six diodes, two capacitors, and auxiliary control unit are all considered critical for the operation, giving the presented RBD. Following this model, the inverter reliability R_{inv} is calculated as the product of the individual component reliabilities, as given in (13). The corresponding inverter failure rate λ_{inv} then equals the sum of the component failure rates, as in (14)

$$R_{inv}(t) = R_{igbt}(t)^6 R_{diode}(t)^6 R_{cap}(t)^2 R_{ctr}(t) \tag{13}$$

$$\lambda_{inv} = 6\lambda_{igbt} + 6\lambda_{diode} + 2\lambda_{cap} + \lambda_{ctr}. \tag{14}$$

Fig. 14 provides the HL2 analysis of the propulsion drive inverter, assuming constant component failure rates. This figure shows the component reliability(a), inverter reliability (b), and the inverter failure rate (c) as a function of time. Following Fig. 14(a), it is concluded that the IGBT is the most fragile part of the inverter. This vulnerability significantly compromises the converter's reliability, as shown in Fig. 14(b), where R_{inv} decreases 5% in less than 2.2 y.

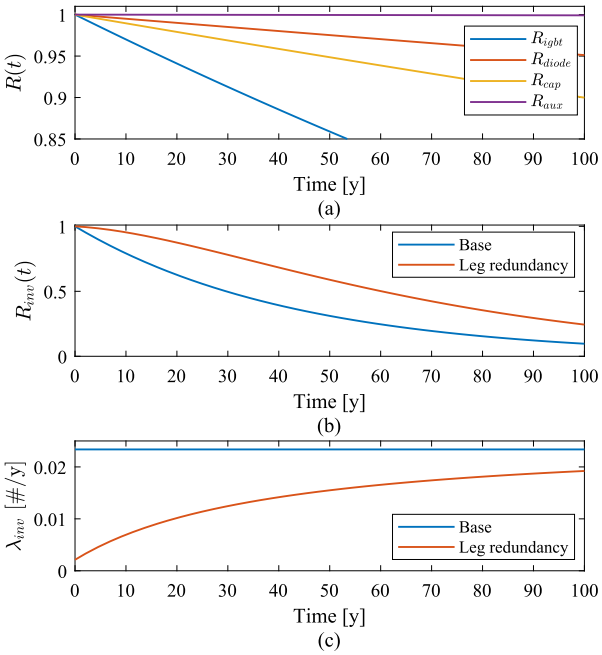

FIGURE 14. Reliability and failure rate curves of the two-level drive inverter and its components. Modeled with and without a redundant phase-leg.

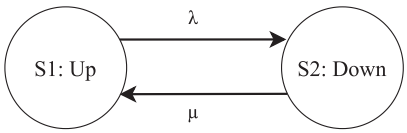

FIGURE 15. Two-state Markov model of a repairable device.

As the propulsion system is consider critical for the vessel operation, the drive inverters must be highly reliable devices. A common method to achieve this target is to add redundancy for the fail-prone components in a device [108], [109]. An example of this is provided in [127], where the Errabelli and Mutschler [127] proposed the use of a redundant phase-leg that can recoup the inverter functionality after a single-leg failure. Assuming independent open-circuit IGBT and diode faults, the inverter's reliability and failure rate curves are changed as given in Fig. 14(b) and (c). It is observed that the leg redundancy significantly lowers the failure rate curve and enhances the inverter's reliability, delaying the 5% drop in R_{inv} from 2.2 to 10.6 y.

While individual components were assumed to be unrepairable, devices can often be repaired. Therefore, the repair process can be added to the two-state Markov model of Fig. 12 as presented in Fig. 15 [113]. In this stochastic model, a device can either function in the *Up* state ($S1$) or fail in the *Down* state ($S2$). In addition to the up-to-down state transition with failure rate λ the device has a down-to-up state transition with repair rate μ. For common devices, μ is considerably higher than λ, causing the MTTR $= 1/\mu$ to be small in comparison to the MTTF $= 1/\lambda$. Upon entering a state, the probability of

TABLE 6. Component Device Reliability Indices for SPS Applications

Device type:	Fault:	λ in [#/y]		μ in [#/h]	
Transmission line	Active	λ_{ta}	0.01	μ_{ta}	0.125
Converter	Passive	λ_{cp}	0.006	μ_{cp}	1
	Active	λ_{ca}	0.006	$\mu_{c,a}$	1
CB	Passive	λ_{bp}	0.01	μ_{bp}	0.25
	Active	λ_{ba}	0.01	μ_{ba}	0.25
	Stuck	f_{cb}	5 %	μ_{bs}	1

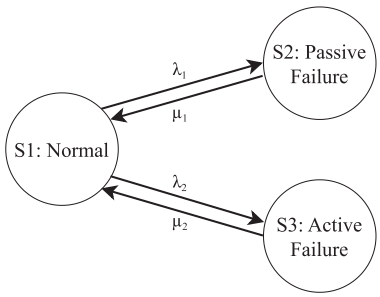

FIGURE 16. Three-state Markov model of a repairable device with active and passive failure modes.

remaining in that state can be described by the exponential (3), where μ is substituted for λ in state $S2$. The state probabilities $P_{S1,S2}$ are governed by the state transition rate matrix (15). Solving these differential equations for equilibrium defines the probability of finding a device in the *Up* state as (16) and in *Down* state as (17), representing the device's availability and unavailability, respectively

$$\begin{bmatrix} P'_{S1}(t) & P'_{S2}(t) \end{bmatrix} = \begin{bmatrix} P_{S1}(t) & P_{S2}(t) \end{bmatrix} \begin{bmatrix} -\lambda & \lambda \\ \mu & -\mu \end{bmatrix} \tag{15}$$

$$P_{S1} = A = \frac{\mu}{\mu + \lambda} \tag{16}$$

$$P_{S2} = U = \frac{\lambda}{\mu + \lambda}. \tag{17}$$

In contrast to using the component failure statistics to model the device reliability, the reliability of SPS devices can also be derived from historical failures or independent testing, like device power cycling tests [128], [129]. For shipboard applications, some typical device reliability indices are given in Table 6, as proposed in [20], [77], and [130]. These indices are derived from manufacturer data and independent testings [131], [132], [133]. Table 6 contains the device failure and repair rate $\{\lambda, \mu\}$ for the transmission lines, converters, and CB. As a device (e.g., PE converter) is constructed by interconnecting components (IGBTs, diodes, and capacitors), it can encounter multiple failure modes. Therefore, Table 6 makes a distinction between active and passive failures. As introduced in [134], a passive failure is represented by an open circuit, which does not impact the remaining healthy devices in the system. In contrast, an active failure acts like a short circuit, causing the fault to propagate from the device through the adjacent power lines and tripping the neighboring protection devices. Optimally, a CB would always trip upon detecting an active fault. However, practically, in about 5% of the cases, the CB is stuck or fails to act accordingly, causing the fault to propagate further into the SPS [20].

The active and passive device failure modes can be combined and modeled using a three-state Markov model, as shown in the state space diagram of Fig. 16. The stuck CB failure mode is modeled as stochastic event that can occur upon an active failure of a neighboring device. This modeling framework is more elaborately discussed in [77].

E. SUBSYSTEM RELIABILITY

Revisiting Fig. 1, it is observed that a SPS can contain several distinct subsystems, each dedicated to a specific function within the vessel. Subsystems like the propulsion system, ESS, radar system, and board net can contain one or multiple PLMs that acquire power from one or multiple PGMs. These modules are then interconnected through numerous devices, like PCMs and dc cables, which can also be shared among the subsystems. An example of a subsystem in Fig. 1 is the propulsion subsystem, which contains the three generators, three rectifiers, two drive inverters, two propulsion motors and the dc bus.

Based on the device reliability analysis (HL2), the reliability of a subsystem can be determined. This HL3 analysis models the functional interdependence of the devices in supplying power to the load modules. The results reflect the ability of the subsystem to meet the power demands throughout the vessel's mission [115], [121]. Besides the adequacy assessment, HL3 analysis provides a framework for analyzing system-level tradeoffs in the SPS design [38].

Fig. 17 gives an overview of the common subsystem-level reliability assessment methods posed in literature. Following this figure, the system-level assessment can be divided into two main categories: the deterministic methods and the probabilistic methods [113]. In a deterministic method, the power system performance is studied under a single or a set of failure scenarios, often reflecting the system's worst-case operating conditions. Under these scenarios, the system must maintain a minimal level of performance, effectively meeting a deterministic design criterion. An example is the N-1 redundancy criterion, which defines that the system must remain fully functional under a single device failure. More generally, the N-M redundancy criterion requires the system to maintain full functionality under M device failures. The N-1 redundancy approach is commonly used to ensure the functionality of key elements in the SPS design. Following the guidelines of [86], the propulsion subsystem in a dynamic positioning vessel of class DPS-3 must incorporate redundancy to maintain fully operational under first-order faults. Alternatively, in [135] RP(3,x) class vessels were proposed where the SPS is required to provide x% of the maximum propulsion power under first-order failures. For transportation vessels, this partial

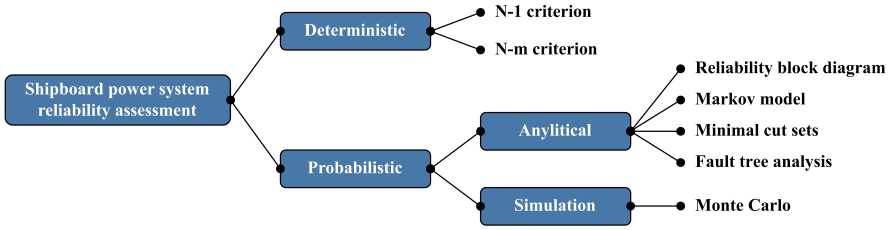

FIGURE 17. Overview of the subsystem reliability assessment methods used to evaluate SPSs.

redundancy is commonly implemented as 50% redundancy where the propulsion system must operate at a minimum of half its rated power in case of a single device fault [136].

Alternatively, the subsystem reliability assessment can be performed using a probabilistic method. With this method, the impact of a large set of failure scenarios is studied and summarized into a single reliability index (or multiple indices) [113]. Unlike deterministic methods, the probabilities of the scenarios are included in the analysis, causing frequent events to contribute more heavily to the reliability index value. So, the probabilistic evaluation recognizes both the severity and likelihood of system failures, thereby including the random nature of the power system in the analysis. As a result, this method provides a more realistic analysis, creating indices that represent actual system risk [137].

In line with Fig. 17, the probabilistic methods can be further divided into analytical methods and simulation methods [109]. In an analytical method, the SPS is represented by a mathematical model that is evaluated to provide numerical results from which the reliability index value can be calculated [113]. These analytical methods provide the benefit of a short computation time for evaluating the index and give insight into the input–output relation of the system. However, these analytical models require significant assumptions, especially for larger more intricate SPSs. Simulation methods, on the other hand, estimate the reliability index value by simulating a detailed model of the SPS. This simulation incorporates the actual operating process and includes the system's random failure behavior. The index value is determined based on a large set of simulation evaluations, treated as a series of experiments. Although more computationally intensive, the simulation method provides significant advantages such as estimating the distributions of a reliability index, incorporating nonelectrical system factors such as the weather effects in the assessment, and including the impact of system processes like reconfiguration, maintenance, and protection [137].

To further compare the probabilistic reliability assessment methods when applied to a shipboard power subsystem, the remainder of this section addresses the most common analytical and simulation methods. This is done by applying each method to a simplified propulsion subsystem of the radial SPS, as given in Fig. 18. Next the appropriate reliability formula are derived, revealing the merits and demerits of each method. The considered subsystem contains two propulsion motors fed from two generators via two rectifiers, two inverters, and a bus-tie CB. For this example, it assumed that the vessel can function on a single motor using a single generator.

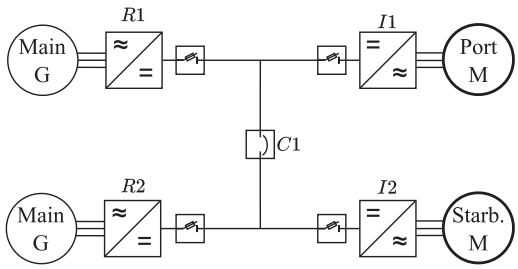

FIGURE 18. Simplified model of the radial shipboard propulsion subsystem.

1) RELIABILITY BLOCK DIAGRAM

The RBD or reliability network was already introduced for modeling the propulsion drive inverter in Fig. 13. This analytical method models the power system as a combination of series and parallel connected blocks, each representing the reliability/availability of a single device [113]. For (nonredundant) series systems, all devices must be functional to achieve system success. Meanwhile, (fully redundant) parallel systems require only one functional device for system functionality. Consequently, the availability of a series and parallel system can be defined as (18) and (19), respectively. With the unavailability $U = 1 - A$

$$A_{\text{series}}(t) = \prod_{i=1}^{N} A_{\text{i}}(t) \tag{18}$$

$$A_{\text{parallel}}(t) = 1 - \prod_{i=1}^{N}(1 - A_{\text{i}}(t)) = 1 - \prod_{i=1}^{N} U_{\text{i}}(t). \tag{19}$$

In the literature, the RBD method is widely used to assess the reliability of power systems. Menis et al. [138] applied the RBD method to a radial MVAC SPS topology. In [139], the method is used to compare the reliability of a unipolar and bipolar MVDC system, while Li et al. [140] used it to model the reliability of meshed HVDC grids. Fig. 19 provides the RBD model for the simplified propulsion subsystem, which is a combination of series and parallel connected device blocks. Notice that the RBD model does not necessarily have the same topological structure as the power system. This, as the RBD model depends heavily on the system requirements and the

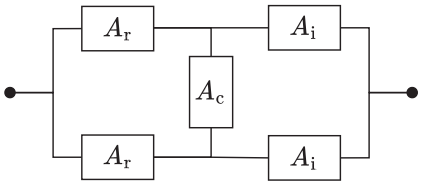

FIGURE 19. RBD for the radial propulsion subsystem.

device functionalities [108]. Applying network reduction to the model gives (20) for the power system availability A_s

$$A_s = A_c((1-U_r^2)(1-U_i^2)) + U_c(1-(1-A_rA_i)^2). \quad (20)$$

2) MARKOV MODEL

As introduced for the device reliability, a Markov process can model the stochastic behavior of a time-varying system using a set of system states [108]. Each state corresponds to a unique system configuration (a set of failed and functioning devices), while transitions between these states are governed by the device's failure and repair rates [38]. For the Markov model to be applicable, the system's behavior must have a lack of memory, implying that future state transitions only depend on the current state of the system.

Fig. 20 provides half of a Markov model for the simplified propulsion subsystem where all devices are allocated a "0" when functional and a "1" when failing. As the propulsion subsystem is composed of five devices, the Markov model contains 2^5=32 states $\mathbb{S} = \{S0, \ldots, S31\}$. Following the propulsion system requirements, the subsystem is failing in 16 states $\mathbb{S}_{\text{Down}} = \{S3, S7, \ldots, S31\}$ while functioning in the other 16 $\mathbb{S}_{\text{Up}} = \{S0, S1, \ldots, S22\}$. To calculate the availability of the propulsion subsystems, the state probabilities $\boldsymbol{P}(t)$, as given in (21), must be calculated

$$\boldsymbol{P}(t) = \begin{bmatrix} P_0(t) & P_1(t) & \cdots & P_{31}(t) \end{bmatrix}. \quad (21)$$

Following Fig. 20, the transition rate α between the states are governed by the device failure and repair rates $\{\lambda, \mu\}$. Defining $\alpha_{i,j}$ as the transition rate from state S_i to S_j, imposes $\alpha_{0,1} = \lambda_{\text{inv}}$ and $\alpha_{1,0} = \mu_{\text{inv}}$[141]. Completing all state transitions provides the transitions rate matrix $\mathbb{A}$ as follows:

$$\mathbb{A} = \begin{bmatrix} \alpha_{0,0} & \alpha_{0,1} & \cdots & \alpha_{0,31} \\ \alpha_{1,0} & \alpha_{1,1} & \cdots & \alpha_{0,31} \\ \vdots & \vdots & \ddots & \vdots \\ \alpha_{31,0} & \alpha_{31,1} & \cdots & \alpha_{31,31} \end{bmatrix} \qquad \alpha_{i,i} = -\sum_{\substack{j=0 \\ j\neq i}}^{31} \alpha_{i,j}. \quad (22)$$

The state probabilities $\boldsymbol{P}(t)$ of the Markov model must follow the Kolmogorov forward equation as given in (23) [141]. To determine the steady-state solution $\boldsymbol{P}(\infty)$ of the Markov process, $\boldsymbol{P}'(t)$ is assumed to be zero. Combined with the fact that $\sum_{i=0}^{31} P_i = 1$, it defines a set of linear equations that can be solved to determine the steady-state probabilities

$$\boldsymbol{P}'(t) = \boldsymbol{P}(t) \cdot \mathbb{A}. \quad (23)$$

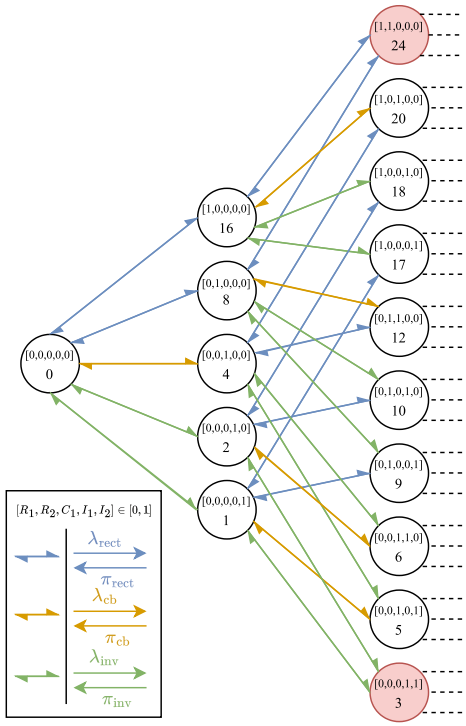

FIGURE 20. Markov model for the radial propulsion subsystem.

The time-dependent solution of (23) can be found using Laplace transforms or by utilizing the standard solution of [141] given in (24). In which $\boldsymbol{P}(0)$ denotes the initial state condition of the subsystem

$$\boldsymbol{P}(t) = \boldsymbol{P}(0) \cdot e^{t\mathbb{A}}. \quad (24)$$

Having obtained the state probabilities, the subsystem availability and unavailability are calculated using the following:

$$A_s(t) = \sum_{s\in\mathbb{S}_{\text{Up}}} P_s(t) \qquad U_s(t) = \sum_{s\in\mathbb{S}_{\text{Down}}} P_s(t). \quad (25)$$

Like RBD, the Markov model method is widely addressed in literature to assess system-level reliability. In [107], the reliability of a shore-to-ship fast charging system is analyzed using Markov chain analysis. Besides considering "up" and "down" states, the authors also introduce partial functioning states. In [142], the Markov method is used to model the reliability of hybrid shipboard power. The authors included the operation profile in the analysis by considering operation mode-specific transition rate matrices $\mathbb{A}_t$.

3) MINIMUM CUT SETS

A MCS is defined as a set of devices whose simultaneous failure leads to a system failure, while a repair of any of the device restores the system's functionality [108]. It effectively represents the smallest combination of device failures that lead to a system failure. The MCS method provides the benefit

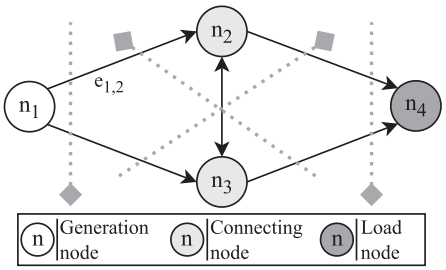

FIGURE 21. Minimum cut sets model for the radial propulsion subsystem.

TABLE 7. Minimum Cut Sets for the Propulsion Subsystem Example

MCS name:	MCS edges:
C_1	$e_{1,2}$ / $e_{1,3}$
C_2	$e_{2,4}$ / $e_{3,4}$
C_3	$e_{1,2}$ / $e_{2,3}$ / $e_{3,4}$
C_4	$e_{1,3}$ / $e_{2,3}$ / $e_{2,4}$

of being fast and efficient to implement digitally while giving insight into the system's distinct failure modes [108].

Fig. 21 provides the directed graph model of the simplified propulsion subsystem. This graph consists of a generation node $n1$, two connection nodes $n2$ and $n3$, and a load node $n4$ all connected through edges $\{e_{1,2}, \ldots, e_{3,4}\}$ [143]. The nodes in the graph represent one terminal devices (e.g., the bus-bars), while the edges characterize the two terminal devices (e.g., rectifiers) that are prone to failures. To deduce the MCS of the propulsion subsystem, the minimum paths algorithm can be applied to the graph, as proposed in [144]. Using this method, the four MCS of the propulsion subsystem are defined as in Table 7 and presented as the dotted lines in Fig. 21. Having obtained the MCS, the unavailability of the subsystem can be approximated as follows [108]:

$$U_s \approx \sum_{i=1}^{4} \left(\prod_{e \in C_i} U_e \right) = U_r^2 + U_i^2 + 2U_r U_c U_i. \tag{26}$$

In [143], MCS is used to evaluate the reliability of a zonal SPSs while Dubey and Santoso [145] used the same approach for the availability calculation and optimization of a shipboard distribution network. Stevens and Santoso [93] applied MSC to assess fundamental segments in utility power systems, while Yu et al. [101] applied the method to analyze electric aircraft.

4) FAULT TREE ANALYSIS

FTA is another analytical method that can be used for the adequacy assessment of SPSs. This method uses boolean operators to represent the relation between the top event (a system failure) and the basic events (the device failures) [113]. FTA was initially developed for the qualitative failure assessment of complex systems as it revealed the cause-effect relation between individual device faults and the system interruption [108]. Later, FTA was used for quantitative reliability evaluations by logically combining the probabilities of basic events to assess the top event.

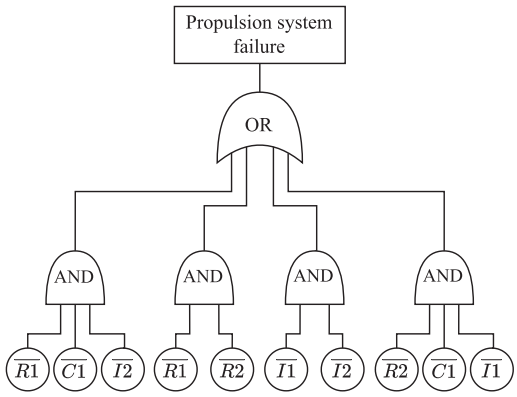

FIGURE 22. Fault tree model for the radial propulsion subsystem.

Fig. 22 provides the fault tree model of the simplified propulsion subsystem, in which a simultaneous supply interruption of the two propulsion motors is considered the top event. Using a set of logic gates {OR,AND,XOR,...}, this top event is gradually broken down into smaller events, eventually reaching the device-level [108]. For constructing the fault tree, other methods, such as RBD and MCS, can be used to determine the failure event combinations.

For the quantitative assessment of the top event, two methods are commonly considered in literature: the Boolean algebra approach and the direct numerical approach [108], [113]. By applying Boolean algebra to the fault tree, the top event is expressed as a combination of unions and intersections of individual device failures. For the propulsion subsystem example, the failure probability is defined as in (27). Using the union rule for probability and assuming independent device failures can simplify the subsystem failure probability of (27) into (28). This transformation moreover uses the definition of unavailability as the steady-state probability of a device failure: $U_r = P[\overline{R_x}]$, $U_i = P[\overline{I_x}]$, and $U_c = P[\overline{C_x}]$

$$P[\overline{S}] = P\left[(\overline{R}_1 \cap \overline{R}_2) \cup (\overline{I}_1 \cap \overline{I}_2) \cup (\overline{R}_1 \cap \overline{I}_2 \cap \overline{C}_1) \cup (\overline{R}_2 \cap \overline{I}_1 \cap \overline{C}_1)\right] \tag{27}$$

$$P[\overline{S}] = U_r^2 + U_i^2 + 2U_r U_c U_i - U_r^2 U_i^2 - 2U_r^2 U_c U_i - 2U_r U_c U_i^2 + 2U_r^2 U_c U_i^2. \tag{28}$$

Like the RBD method, the Boolean algebra approach provides the exact failure probability of the subsystem. However, this comes with the downside of solving a complex Boolean expression, especially for evaluating larger power systems [108]. Alternatively, the direct numerical approach evaluates the probability values at the different levels of the fault tree rather than deferring this evaluation till the top event. The resulting subsystem failure probability is provided in (29), which

matches the probability defined in (26) when assuming independent device failures

$$P[\overline{S}] = P\left[\overline{R}_1 \cap \overline{R}_2\right] + P\left[\overline{I}_1 \cap \overline{I}_2\right] + P\left[\overline{R}_1 \cap \overline{I}_2 \cap \overline{C}_1\right] + P\left[\overline{R}_2 \cap \overline{I}_1 \cap \overline{C}_1\right]. \quad (29)$$

Vicenzutti et al. [146] use a fault tree to assess the reliability of an all-electric drillship powered using a three-segment ring ac-SPS. The top event is defined as the "loss of load supply capability," which considers the vessel's operating mode. In [147], FTA is used to determine the emergency switchboard reliability of a nuclear vessel with a radial SPS topology. Others use FTA to analyze the impact on the SPS adequacy of the power system topology [77], added power lines [20], and the third power system dimension [148].

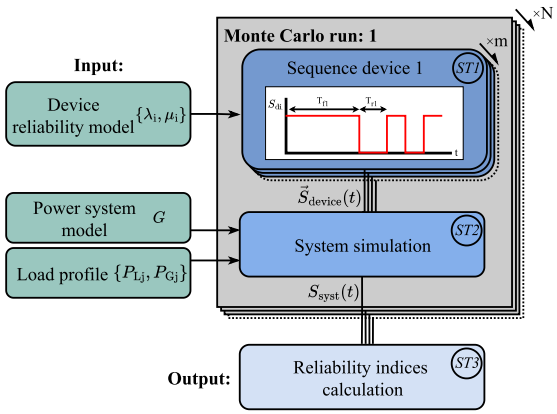

FIGURE 23. Proposed MC framework for reliability assessment of dc-SPSs.

5) MONTE CARLO

While analytical methods use mathematical models to evaluate the SPS reliability, the MC method estimates the reliability index value through a set of simulation evaluations, also known as trails or experiments [108], [149]. These simulations emulate the operating process of the SPS while incorporating its stochastic failure behavior. The uncertainty in device functionality is modeled using a set of RV, which are governed by probability distributions [109], [150]. Throughout the simulations, these RVs are repeatedly sampled, representing the randomness in device failures and repairs. The result of each simulation is then compiled into a reliability index sample. The MC concept is based on the law of large numbers, which dedicates that the average of a large number of RV realizations converges to the expected value [151]. Therefore, when the number of simulations N is large enough, the average of the reliability index samples converges to the expected value, accurately reflecting the system's adequacy

Hence, the MC method requires an extensive number of simulation runs to determine the reliability index value, making it computationally intensive when compared to an analytical approach that often uses a single equation for reliability evaluation [113]. However, when considering larger and more intricate power systems, these analytical methods become difficult to apply and require significant assumptions to deal with the complex operating conditions. MC simulation, on the other hand, can incorporate a more detailed SPS model to cope with the system complexity. This model intricacy moreover provides flexibility in design, making the reliability comparison of SPS topologies simpler and more accurate. Besides the model accuracy, the MC method provides other advantages that can be defined as follows [137].

1) MC simulation can simultaneously estimate the expected value and the distributions of a wide range of reliability indices, which analytical methods generally cannot.
2) The MC simulation can include the impact of system processes, such as reconfiguration, maintenance, and protection, which may have to be approximated analytically.
3) MC simulation can incorporate nonelectrical system factors, such as weather effects and staff availability in the assessment.

As introduced in [113], a MC method for power systems reliability analysis consists of three main steps: device failure sampling $ST1$, system simulation $ST2$, and reliability index calculation $ST3$. Depending on the device failure sampling, a distinction can be made between a nonsequential and a sequential MC simulation. In a nonsequential method, the operation time is not considered, causing the device functionalities to be sampled from their availabilities while the load profile of the power system is sampled from its probability distribution. Meanwhile, the sequential approach simulates the power system in chronological order, sampling a device's time-to-failure and time-to-repair while considering a time scenario like a three-month operating load profile of the vessel. Li et al. [137] proposed three simulation approaches for the reliability evaluation of power systems: state sampling, state duration sampling, and state transition sampling. An example of a sequential MC method based on the state duration sampling approach for the SPS reliability assessment is provided in Fig. 23.

As observed in Fig. 23, step $ST1$ uses the device failure and repair rates $\{\lambda_i, \mu_i\}$ to create the failure sequence samples $S_{di}(t)$ of the m devices in the SPS. These time series are constructed as a concatenation of RV realizations, representing an alternation of the time-to-failure $T_f \sim Exp(\lambda_i)$ and time-to-repair $T_r \sim \text{Exp}(\mu_i)$ samples. Once a failure sequence has been sampled for all m devices, defining $\vec{S}_{device}(t)$, the system functionality is simulated. $ST2$ considers the SPS layout using the graph model G and applies active fault propagation to the power system model. Moreover, it evaluates the system performance $S_{syst}(t)$ given the requirements and operation load profile $\{P_{Lj}, P_{Gj}\}$. Finally, $ST3$ calculates the reliability index estimates based on the N simulation evaluations.

Applying the MC method of Fig. 23 to the simplified propulsion subsystem provides an estimate of the probability of subsystem functionality $\hat{P}_{syst}(t)$ as defined in (30). In this equation, N is defined as the number of simulation runs, and

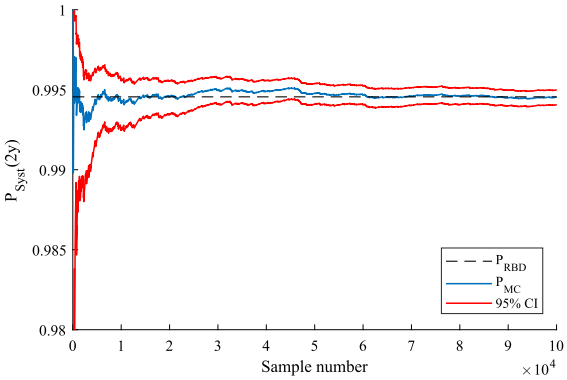

FIGURE 24. Simplified MC simulation for the propulsion subsystem with considering open circuit device failures with $A_c = 0.9$ and $A_{r,i} = 0.95$.

k is the number of times the system was functional at time t. Note that besides $\hat{P}_{\text{syst}}(t)$, many other reliability indices can be derived from $S_{\text{syst}}(t)$, such as the service interruption rate, total downtime per year, MTBSI, and the Bx-lifetime

$$\hat{P}_{\text{syst}}(t) = \frac{k}{N}. \tag{30}$$

For comparison, it is assumed that the devices in the propulsion subsystem can encounter solely open circuit failures with a device availability of $A_c = 0.9$ and $A_{r,i} = 0.95$. The result of the MC simulation is provided in Fig. 24, which shows $\hat{P}_{\text{syst}}(2y)$ as a function of N. From this figure, it is concluded that the MC estimate approximates the RBD availability of (20) when N is larger than 50 k. Moreover, in line with the law of large numbers, it is observed that the variability of the estimate reduces as N increases.

For the calculation of $\hat{P}_{\text{syst}}(t)$, an additional simulation run has either a functional (k+1) or nonfunctional (k+0) system at time t. This success or failure outcome cause the results to be treated as a Bernoulli experiment. Therefore, a CI for the true probability of subsystem functionally $P_{\text{syst}}(2y)$ can be defined using the exact CI method as proposed in [113]. The $(1-\alpha)$ CI can defined as in (31) in which $P_{\text{syst},u}$ and $P_{\text{syst},l}$ are defined as the upper and lower interval bound, respectively. Fig. 24 shows the convergence of the interval for a 95% ($\alpha = 0.05$) confidence level

$$\begin{aligned} P_{\text{syst},u} &= 1 - \text{betainv}\left(\frac{\alpha}{2}, N-k, k+1\right) \\ P_{\text{syst},l} &= 1 - \text{betainv}\left(1-\frac{\alpha}{2}, N-k+1, k\right). \end{aligned} \tag{31}$$

Zhang et al. [152] propose a hierarchical reliability framework based on a nonsequential MC simulation to determine the system-level reliability while incorporating the PE converter reliability. Similarly, Rei and Schilling [153] used MC simulation to estimate the contingency level probability of the Brazilian transmission system while Shahidirad et al. [154] applied the method to determine the probability of functionality in a PV system. Finally, Sankarakrishnan and Billinton [155] used a sequential MC simulation to evaluate the composite generation and transmission system reliability on the six-bus RBTS model.

6) METHOD COMPARISON

While the five probabilistic methods all yielded a subsystem reliability index estimate, the evaluation process revealed the merits and demerits of each method. The RBD and MCS methods provided a fast estimation of the system availability. However, both required significant assumptions to cope with complex operating conditions. MSC and RBD use modeling assumptions like no active device failures or system-level reconfiguration, which result in inaccurate modeling of fault-tolerant power systems [38]. Using FTA or Markov models allows the reliability assessment to include active device failures and the fault protection system. However, for these methods, the number of system states increases exponentially with the power system size. This makes a Markov model or FTA optimal for evaluating small-sized SPSs, though the assessment complexity rises significantly when addressing larger intricate power systems. The MC method, on the other hand, can incorporate a more detailed model of the SPS while maintaining flexibility and versatility in the assessment. Meanwhile, the simulation model can include system processes like reconfiguration, maintenance, and protection in the reliability assessment. Hence, the MC method provides an accurate estimate of a broader range of reliability indices, making the reliability assessment of complex SPSs with intricate redundancies simpler and more accurate. However, compared to analytical methods, MC demands a significantly higher computational effort, especially when high accuracy is required [153].

Table 8 provides an overview of the relevant studies considering subsystem-level reliability assessment methods. This table shows each publication's reliability class, method, goal, and the considered reliability indices. Moreover, it provides an overview of each study's application, grid topology, and research focus. The table aims to highlight the state-of-the-art in adequacy assessment of SPSs while revealing the gaps for future reliability research. From Table 8, it can be concluded that most of the current SPS reliability assessments are achieved through an analytical strategy. Here, a method like RBD is more commonly used to assess the less intricate radial and ring topology, while the zonal and BAAH are primarily evaluated using the FTA method in combination with Markov modeling. In addition, it is concluded that the MC method is more commonly applied when assessing larger meshed power systems.

The optimal method for evaluating the SPS reliability depends strongly on the vessel's complexity and the reliability target. This target (a goal or requirement) imposes a set of "to be addressed" reliability indices and their required accuracy level. These considerations guide the level of simplification allowed for the device and system models, as well as the system operation assumptions. Understanding the vessel complexity and the reliability target thus provides preference in

TABLE 8. Studies on probabilistic reliability assessment of power systems.

Publications on probabilistic reliability analysis							
Class:	**Method:**	**Reliability goal:**	**Indices:**	**Application:**	**Topology:**	**Focus:**	**Ref:**
Analytical	RBD	Assessment	• System condition	AC SPS	Radial	Using the decomposition of the IPS, a RBD and dynamic RBD are designed to evaluate the reliability of the IPS.	[138]
		Comparison	• SAIDI	Utility grid	Radial Ring	Determine the impact of different dc grid concepts on the reliability of a monopolar, bipolar, and hybrid configuration.	[139]
		Assessment	• System reliability	HVDC grid	Ring	Modeling and comparing the reliability of LCC and LCC/VSC hybrid HVDC grids, using a hierarchical MMC model to assess the impact of redundancy.	[140]
	Markov model	Assessment	• System failure prob.	DC SPS	Radial	Using a multi-phase Markov model, the reliability of a radial SPS is determined considering the vessel's operation modes.	[142]
		Assessment	• LOCE • DCE	Shore-to-Ship Charging	Radial	Determine the reliability of a shore-to-ship charging systems, using a multilayer Markov based framework.	[107]
	Minimum cuts sets	Assessment	• System interruption rate • Probability gain	DC SPS	Zonal	Determine the service interruption rate of all SPS loads and the probability gain under a faulty segment.	[143]
		Assessment	• MTTR • Total downtime • Failure rate	Utility grid	Ring Zonal BAAH	Determines the reliability of fundamental substation segments by using active, passive, and stuck component failures.	[93]
		Minimal level	• System interruption rate • Availability • MTTR	SPS	Meshed	Find the optimal in-zone distribution topology with the minimal number of edges that achieves the set availability level.	[145]
		Assessment	• System reliability	Elect. aircraft	Radial	Modeling the reliability of a more electric aircraft from the component level to the system level.	[101]
	FTA	Assessment	• System failure prob.	AC SPS	Radial	Using fault tree analysis, the probability of emergency system failure is obtained, and the importance index of the loads.	[147]
		Assessment	• System interruption rate	3D DC SPS	Zonal	Analyze the impact of the third dimension on the reliability of the SPS.	[148]
		Assessment	• System interruption rate • MTTR	DC SPS	Zonal BAAH	Determine the reliability indices of different BAAH topologies for multiple subsystems in the vessel.	[77]
		Improvement	• System interruption rate	DC SPS	BAAH	Using PSO optimize the placement of additional busses in the BAAH topologies maximizing the SPS reliability.	[20]
		Improvement	• System interruption rate • System cost	DC SPS	BAAH	Providing a framework for optimizing the SPS reliability by comparing topologies and improving the in-zone distribution.	[130]
		Improvement	• System interruption rate • Availability • Expected lifetime fails	AC SPS	Ring	Providing a new SPS design process that integrates quantitative reliability analysis and dynamic system modeling.	[146]
Simulation	MC	Comparison	• LOLE	Utility grid	Meshed	Two Monte Carlo models are compared in terms of convergence and computation speed.	[156]
		Assessment	• System failure prob.	Utility grid	Ring	Determine the reliability of a three-bus grid and compare to the analytical result	[157]
		Comparison	• Prob. of curtailment • EFLC • EENS	Utility grid	Meshed	Monte Carlo based composite power system reliability assessment using antithetic variates to reduce the simulation variance.	[155]
		Impact determination	• EENS • LOLE	Utility grid	Meshed	Using MC simulation and ML regression techniques, determine the impact of the RES PE converter reliability on the power system level reliability	[152]

the method selection. For instance, if the reliability goal is to determine the long-term impact of full redundancy on the SPS, the RBD or MCS method can provide a good estimate at a low effort. However, when studying the impact of the fault protection on the system level reliability, a Markov or MC method is preferred. In general, if the complex operating conditions of a SPS are not considered and/or the system failure probability is very low (extremely reliable SPS), the analytical techniques are often preferred over MC simulation [137]. However, following [153], the analytical and simulation methods can be used complementary, suggesting that the optimal reliability method can be a combination of multiple.

F. SYSTEM RELIABILITY

The final step in the reliability assessment of a SPS is the HL4 analysis, which combines the adequacy performance of the different subsystems to define the system-level reliability. This reliability figure is crucial for analyzing system-level design tradeoffs or optimizing the power system design for reliability. An example of the HL3 to HL4 step is given in (32) as proposed in [20], where the system failure rate is defined as a linear combination of the subsystem failure rates with the coefficients representing the relative criticality of a subsystem in the vessel

$$\lambda_{\text{syst}} = 1.5(\lambda_{\text{radar}} + \lambda_{\text{pulsed}}) + \lambda_{\text{prop.}} + 0.5(\lambda_{\text{ess}} + \lambda_{\text{zones}}). \tag{32}$$

While optimizing the SPS design for (32) results in a minimal system interruption rate, following Section III-A, this was considered to be a suboptimal outcome as the load characteristics are ignored. Therefore, when analyzing the complete SPS reliability, it is essential to include a combination of multiple subsystem reliability indices that reflect the different load types.

IV. RELIABILITY IMPROVEMENT

In Section II, it was established that the design of a SPS affects multiple performance metrics of the vessel, including the affordability, efficiency, simplicity, power density, reliability, and survivability. Focusing on reliability, Section III presented several probabilistic methods for evaluating the power system adequacy. However, despite careful design and assessment, certain SPSs may fail to meet the predefined reliability requirements. Alternately, for some unique vessel applications,

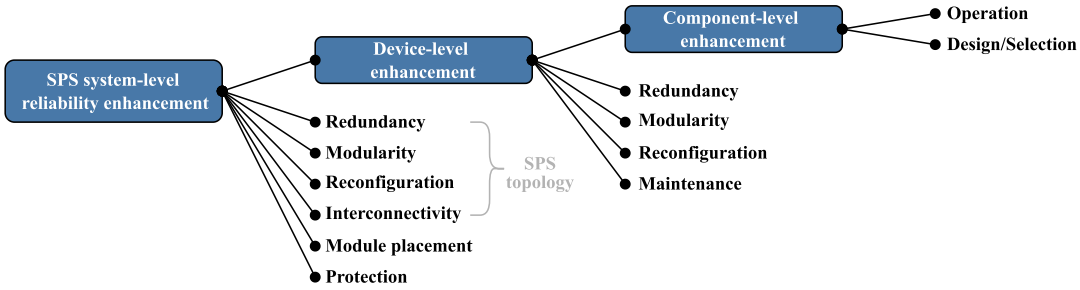

FIGURE 25. Overview of the system reliability improvement methods.

an exceptionally high supply adequacy can be necessary for powering critical loads. In those cases, several techniques may be employed to enhance the SPS's reliability.

Following the hierarchical reliability framework of Fig. 9, a power system reliability enhancement is achieved either directly via system-level changes or indirectly via a component-level or device-level improvement. Fig. 25 provides an overview of the conventional methods used to improve the power system reliability. This figure subdivides the improvement methods into system-level, device-level, and component-level reliability enhancements.

A. SYSTEM-LEVEL ENHANCEMENTS

System-level methods enhance power system reliability through changes in power system design while maintaining the reliability of devices and components. Examples of system-level methods are: redundancy, modularity, reconfiguration, interconnectivity, module placement, and protection.

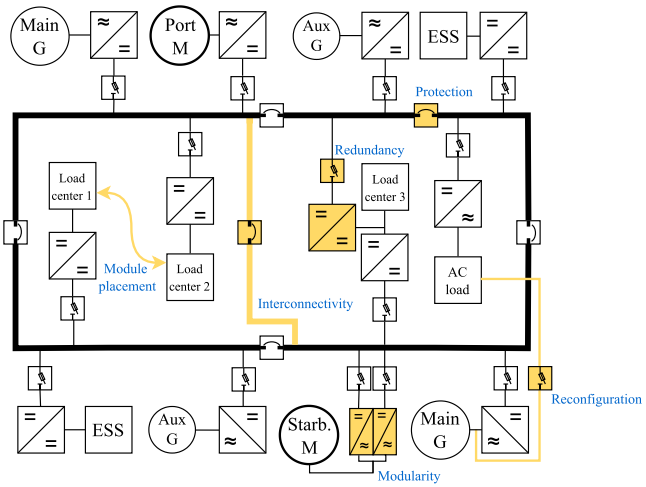

FIGURE 26. Visualization of the system-level reliability enhancement techniques for the ring SPS topology.

1) REDUNDANCY

System-level redundancy is a common method used for enhancing the reliability of a power system [158]. Redundancy involves the incorporation of extra devices or systems to ensure supply continuity even if one fails. This duplication reduces the probability of a device failure leading to a supply interruption, thus enhancing the system's reliability.

Following [19], system-level redundancy can be split into two main types: structural redundancy and functional redundancy. Structural redundancy concerns the incorporation of device duplicates, causing the system to function correctly even if one or several of the duplicates fail. Structural redundancy can be further segregated into active redundancy, where the devices share the function till failure, and passive redundancy, where the function is taken over by a stand-by device only after a failure. An example of structural redundancy for a ring-type DC-SPS is provided in Fig. 26, where load center 3 is powered from two separate switchboards through two fully redundant dc–dc converters. Functional redundancy is considered when two devices perform separate functions in normal operation, though they can take over each other's function in case of a device fault. An example of functional redundancy in SPS applications is a shaft generator that can function as a propulsion motor during engine failure.

The redundancy concept is widely addressed in literature as a way of improving system-level reliability. In [20], the impact of a redundant power line on the service interruption rates of a BAAH SPS is studied. The authors use an additional dc–dc converter and CB to power the pulsed load module in the SPS. The studies concluded that the added redundancy can reduce the service interruption rate of the pulsed load module from 0.06 to 4e-6 #/y. In [159], the impact of redundancy on the reliability of ship machinery systems is analyzed. The authors concluded that using two fully redundant pumps can increase the MTTF by a factor of 100 in the case of single-day voyages.

Even though redundancy can enhance the SPS reliability of a specific subsystem, a complete SPS reliability enhancement is not guaranteed. As observed in [20], the redundant feed-in for the pulsed load module unfavorably increases the service interruption rate of the radar and ESS. This reduced reliability in other parts of the SPS occurs as implementing redundancy requires additional components that enhance the power system complexity and raise the expected number of device failures over the power system lifetime. While redundancy can thus benefit the reliability of a single subsystem, it might come with a reduced adequacy performance for the remainder of the power system.

2) MODULARITY

Another method used to enhance the system-level reliability is modularity. Modularity is defined as the degree to which components/devices are separated into functional modules with minimal levels of interdependence. In the power system context, increasing the level of modularity requires the power system to be constructed of more independent modules that combined achieve the same functionality. An example of increased modularity for SPS applications is provided in Fig. 26, where the starboard propulsion motor is excited through two dc–ac inverters, each capable of providing half the rated motor power. As the two devices operate independently, a failure in one of the devices causes a derated operation instead of a complete motor outage. For some vessel loads, like the propulsion motors, this derated operation can significantly mitigate performance degradation. Generally, the increased level of modularity reduces the system's functional dependence on individual devices, resulting in more gradual performance degradation upon failure events. However, it is essential to note that increased modularity is only considered beneficial if the load can function in a derated mode or when it is combined with redundancy. As modularity can reduce redundancy requirements to maintain a fully rated operation with improved reliability.

Zhaksylyk et al. [160] compared the reliability of a nonmodular ac–dc rectifier with one that uses a three-module structure. Despite the increased component count, the modular converter was found to have a B1 lifetime, a factor 100 higher than that of the nonmodular converter. Mousavizadeh et al. [161] analyzed another type of system-level modularity through the resiliency analysis of a distribution network. In this article, modularity is defined as the system's ability to divide into independent, self-provided subsystems.

3) RECONFIGURATION

Like redundancy and modularity, reconfiguration is a widely applied method for enhancing the reliability of a power system. A system-level reconfiguration is a set of rearrangements or changes made to the power system configuration that adapt the system structure to a new operating condition, aiming to improve the vessel's performance. In SPS applications, a reconfiguration is generally applied post-fault. After detecting a service interruption and isolating the faulty device, the reconfiguration restores and optimizes the vessel's functionality through configuring the CBs and disconnectors [37], [162]. The reconfiguration thus maximizes the supply adequacy in the event of power system faults, thereby enhancing the reliability of shipboard interrupt loads.

The post-fault reconfiguration is considered an optimization problem that can be solved for multiple goals, including power loss minimization [163], stability improvement [164], and reliability maximization [134]. In literature, multiple methods are posed that solve this optimization problem given the reconfiguration goal and power system requirements [165], [166]. Mitra and Venayagamoorthy [167] defined a reconfiguration algorithm for the optimal supply of priority-weighted loads in a ring-type SPS. Amanulla et al. [134] compared a reconfiguration strategy aimed at maximizing system reliability with a strategy that minimizes power loss. For the 33-bus system, it is observed that the more reliable power system configuration reduced the power system downtime and EENS at the expense of the system's efficiency.

An example of reconfiguration for SPS applications is provided in [168], where the configuration of the disconnectors in a zonal-type SPS is changed based on different failure events. An example of added reconfiguration for SPS applications is shown in Fig. 26, where the power feed to the AC load center can be reconfigured from the dc switchboard to a direct ac link connected to the main generator. This reconfiguration fully bypasses the dc distribution in case of a complete power system outage.

Besides the impact on reliability, reconfiguration also benefits the vessel's performance when facing faults imposed by unanticipated environments, such as fires, floods, or missile impacts. By restoring and optimizing the system structure, the reconfiguration strategy improves the post-fault performance of the vessel, thereby enhancing the SPS survivability. Moreover, as proposed in [169], a probabilistic reconfiguration strategy can be employed that changes the power system structure prior to a fault, minimizing the impact of potential failures. This prefault strategy uses reconfiguration to mitigate vulnerabilities in the SPS design for a given operation.

4) OTHER METHODS

Besides the common improvement methods, other system-level strategies are posed in literature that can enhance the adequacy of a SPS. As proposed in [145], the availability of a shipboard distribution system can be enhanced by increasing the network interconnectivity. The authors found that for a 15-node distribution circuit, increasing the number of conductors from the minimum of 14 to the maximum of 22 can reduce the system interruption rate by over a factor of 50 while also lowering the MTTR. An example of increased interconnectivity for SPS applications is provided in Fig. 26, where a power line is added between the two opposite switchboards of the ring-type power system.

An important observation regarding these enhancement methods is that selecting a power system topology, as discussed in Section II-C, inherently determines the baseline levels of redundancy, modularity, reconfiguration, and interconnectivity. Changing the power system design from, for instance, a radial topology to a zonal topology increases the level of redundancy and interconnectivity while allowing for enhanced reconfiguration.

Another reliability improvement strategy posed in literature is the optimization of module placement. An example is provided in Fig. 26, where load center 1 is connected to a switchboard with an ESS and auxiliary generator while load center 2 is paired with a main generator and port side motor. As a result, the supply adequacy of load center 1 will be higher

than that of load center 2. As the two load centers can have different priority levels based on their criticality, optimizing module placement can enhance the full power system reliability. Stevens et al. [20] proposed a module placement algorithm to optimize the configuration of the loads and generators within a BAAH-type SPS. Upon applying the algorithm, the overall system interruption rate was decreased by 0.54% when compared to the base configuration.

A final system-level strategy is improving the fault protection system. As mentioned by Al-Kuwaiti et al. [116], the reliability of a SPS is dependent on its ability to perform fault detection, fault isolation, and system restoration. While reconfiguration was proposed to optimize the restoration process, detection and isolation are the prime focus of the fault protection system [37]. Enhancing the level of protection in a SPS reduces the active fault propagation through the dc network, limiting the fault's impact on the vessel performance. An example of increased fault protection for SPS applications is provided in Fig. 26, where an additional CB is installed to further segment the port-side switchboard. This CB enhances the isolation capability of the SPS, thus improving its reliability. However, as discussed in the introduction, designing a FPS for a dc-SPS is a challenging task due to the significant tradeoffs.

B. LOWER LEVEL ENHANCEMENT

In addition to system-level methods, the reliability of a SPS can be improved indirectly via a component-level or device-level enhancement. These lower level methods use more reliable devices while keeping the SPS structure constant. On a component level, the reliability can be enhanced through either an improved operation or a better component design/selection. For example, an IGBT can be operated with a lower junction temperature to improve its lifetime [38]. Alternatively, the "new dual" IGBT modules that use copper bond wires and silver sintering can be selected to improve the component's reliability performance [170].

Besides improving the component reliability, the reliability of a converter can be enhanced by implementing device-level redundancy, modularity, and reconfiguration. The impact of implementing redundancy and modularity on the converter reliability is considered in [59] for a MMC. For the MMC, increasing the switch voltage rating reduces the level of modularity and enhances the converter reliability. Meanwhile, using more redundant submodules in the MMC benefits the converter reliability. Another device-level method that is often employed to enhance the power system reliability is maintenance. Preventive maintenance of devices can keep the system's reliability above a predefined level. As shown in [101], reducing the periodic maintenance period significantly enhances the adequacy performance of the power system throughout its lifetime.

C. ENHANCEMENT METHOD DEPLOYMENT

Deploying the system-level, device-level, and component-level strategies, as outlined in Fig. 25, can significantly benefit the dc-SPS reliability. However, each method provides a different degree of reliability improvement, where the actual impact also depends on design elements, such as the integration approach, the SPS base configuration, and the vessel's performance requirements. Identifying an optimal strategy for enhancing the SPS reliability is critical for achieving a cost-effective solution. However, a comprehensive quantitative comparison of the enhancement methods has yet to be addressed in literature. To resolve this research gap, the hierarchical model framework of Section III can be used to evaluate the impact of each method on the dc-SPS reliability. Then, offsetting this improvement against the implementation's size, weight, cost, and losses provides the relative effectiveness of each enhancement method. Ultimately, these results will guide the improvement method selection, ensuring a reliable dc-SPS at a minimal cost.

V. CONCLUSION

The AES is a crucial element for realizing future emission targets in the maritime sector. The basis of an AES is the SPS, which serves as the interconnecting grid between the vessel loads and generation modules. While both ac and dc power system can be employed, dc-SPSs offer advantages in efficiency, power density, and ESS integration. However, the enhanced network interconnectivity, high penetration of PE devices, and harsh environmental conditions make reliability assurance a challenging yet critical part of the dc-SPS design. To address this matter, this article provided a comprehensive overview of the reliability aspects of dc-SPSs, considering the design, assessment, and improvement.

While dc-SPSs provide flexibility in the bus configuration and network topology selection, its design was found to retain tradeoffs between the reliability and other performance parameters. Selecting a high bus voltage can benefit the system's efficiency and power transfer capacity but comes with enhanced isolation/safety requirements and increased system complexity. Selecting a bipolar dc bus over a unipolar one can benefit the system's reliability but harm its stability and simplicity. The five discussed power system topologies each provided unique merits and demerits, imposing a performance tradeoff with the topology selection. Implementing a zonal topology benefited the system's reliability and survivability while using a radial topology imposed higher simplicity, efficiency, and power density. Ultimately, the bus design and topology selection are optimization problems that depend on the vessel's application and performance priorities.

The dc-SPS reliability assessment is critical for verifying design specifications and optimizing future adequacy investments. While reliability is defined as a probability measure, many other indices are used to represent load point adequacy. However, with the unique load properties and grid aspect of SPSs, an intricate reliability framework is imposed where specific loads can be shed with a lower impact on the system's performance. Consequentially, the effectiveness of a reliability index depends heavily on the considered load type. To evaluate these indices, a hierarchical reliability model

framework was proposed. This model characterized the dc-SPS reliability from the component level up to the system level. Various subsystem reliability models were introduced, including RBD, Markov, MCS, FTA, and MC simulation. While all methods yielded an index estimate when applied to the subsystem example, the evaluation process revealed the merits and demerits of each method. The optimal method for evaluating the dc-SPS reliability was found to depend on the considered network topology and reliability target. Where analytical methods like RBD and MCS are optimal for the fast assessment of small-sized SPSs, Markov modeling and MC simulation are better for evaluating larger intricate SPSs.

For a designed dc-SPS, several system-level, device-level, and component-level strategies can be deployed to enhance the reliability performance. System-level methods, such as redundancy, modularity, and reconfiguration, enhance the SPS reliability through changes in power system design. While these methods benefit individual subsystems, they often introduce complexities that can undermine the reliability of the overall system. Identifying an optimal deployment of the enhancement methods remains a research gap, yet it is crucial for achieving cost-effective reliable dc-SPS solutions.

REFERENCES

[1] T. Smith et al., "Third IMO GHG study," International Maritime Organization (IMO), Tech. Rep., 2015.

[2] J. Faber et al., "Fourth IMO GHG study," International Maritime Organization (IMO), Tech. Rep., 2020.

[3] M. Cames, J. Graichen, A. Siemons, and V. Cook, "Emission reduction targets for international aviation and shipping," EPRS: European Parliamentary Research Service, Tech. Rep., PE 569.964, 2015.

[4] The Marine Environment Protection Committee, "2023 IMO strategy on reduction of GHG emissions from ships," IMO, Tech. Rep. MEPC.377(80), 2023.

[5] T.-H. Joung, S.-G. Kang, J.-K. Lee, and J. Ahn, "The IMO initial strategy for reducing Greenhouse Gas(GHG) emissions, and its follow-up actions towards 2050," *J. Int. Maritime Saf., Environ. Affairs, Shipping*, vol. 4, no. 1, pp. 1–7, Jan. 2020.

[6] S.-Y. Kim, S. Choe, S. Ko, and S.-K. Sul, "A naval integrated power system with a battery energy storage system: Fuel efficiency, reliability, and quality of power," *IEEE Electrific. Mag.*, vol. 3, no. 2, pp. 22–33, Jun. 2015.

[7] A. Haxhiu, A. Abdelhakim, S. Kanerva, and J. Bogen, "Electric power integration schemes of the hybrid fuel cells and batteries-fed marine vessels-an overview," *IEEE Trans. Transport. Electrific.*, vol. 8, no. 2, pp. 1885–1905, Jun. 2022.

[8] S. Fang, Y. Wang, B. Gou, and Y. Xu, "Toward future green maritime transportation: An overview of seaport microgrids and all-electric ships," *IEEE Trans. Veh. Technol.*, vol. 69, no. 1, pp. 207–219, Jan. 2020.

[9] H. P. Nguyen et al., "The electric propulsion system as a green solution for management strategy of CO_2 emission in ocean shipping: A comprehensive review," *Int. Trans. Elect. Energy Syst.*, vol. 31, no. 11, pp. 1–29, 2021.

[10] J. Hinkle and T. L. Glover, "Reduced manning in DDG 51 class warships: Challenges, opportunities and the way ahead for reduced manning on all united states navy ships," in *Proc. Eng. the Total Ship (ETS) Symp.*, 2004, pp. 1–30.

[11] M. Cupelli et al., "Power flow control and network stability in an all-electric ship," *Proc. IEEE*, vol. 103, no. 12, pp. 2355–2380, Dec. 2015. [Online]. Available: https://ieeexplore.ieee.org/document/7329677

[12] G. Sulligoi, A. Vicenzutti, and R. Menis, "All-electric ship design: From electrical propulsion to integrated electrical and electronic power systems," *IEEE Trans. Transport. Electrific.*, vol. 2, no. 4, pp. 507–521, Dec. 2016. [Online]. Available: https://ieeexplore.ieee.org/document/7530867/

[13] C. Nuchturee, T. Li, and H. Xia, "Energy efficiency of integrated electric propulsion for ships: A review," *Renewable Sustain. Energy Rev.*, vol. 134, Dec. 2020, Art. no. 110145.

[14] J. F. Hansen and F. Wendt, "History and state of the art in commercial electric ship propulsion, integrated power systems, and future trends," *Proc. IEEE*, vol. 103, no. 12, pp. 2229–2242, Dec. 2015.

[15] S. J. Dale, R. E. Hebner, and G. Sulligoi, "Electric ship technologies," *Proc. IEEE*, vol. 103, no. 12, pp. 2225–2228, Dec. 2015.

[16] G. Castles, G. Reed, A. Bendre, and R. Pitsch, "Economic benefits of hybrid drive propulsion for naval ships," in *Proc. 2009 IEEE Electric Ship Technol. Symp.*, Apr. 2009, pp. 515–520.

[17] R. Hebner, "Energy storage on future electric ships," Electric Ship Res. Develop. Consortium, Tech. Rep., 2014.

[18] S. Guo, Y. Wang, L. Dai, and H. Hu, "All-electric ship operations and management: Overview and future research directions," *eTransportation*, vol. 17, Jul. 2023, Art. no. 100251. [Online]. Available: https://www.sciencedirect.com/science/article/pii/S2590116823000267

[19] W. Tarelko, "Redundancy as a way increasing reliability of ship power plants," *New Trends Prod. Eng.*, vol. 1, no. 1, pp. 515–522, Oct. 2018.

[20] B. Stevens, A. Dubey, and S. Santoso, "On improving reliability of shipboard power system," *IEEE Trans. Power Syst.*, vol. 30, no. 4, pp. 1905–1912, Jul. 2015.

[21] M. U. Mutarraf, Y. Terriche, K. A. K. Niazi, J. C. Vasquez, and J. M. Guerrero, "Energy storage systems for shipboard microgrids: A review," *Energies*, vol. 11, no. 12, Dec. 2018, Art. no. 3492.

[22] E. Skjong, R. Volden, E. Rodskar, M. Molinas, T. A. Johansen, and J. Cunningham, "Past, present, and future challenges of the marine Vessel's electrical power system," *IEEE Trans. Transport. Electrific.*, vol. 2, no. 4, pp. 522–537, Dec. 2016.

[23] M. Chai, D. R. Bonthapalle, L. Sobrayen, S. K. Panda, D. Wu, and X. Chen, "Alternating current and direct current-based electrical systems for marine vessels with electric propulsion drives," *Appl. Energy*, vol. 231, pp. 747–756, Dec. 2018. [Online]. Available: https://www.sciencedirect.com/science/article/pii/S0306261918313710

[24] P. Ghimire, M. Zadeh, J. Thorstensen, and E. Pedersen, "Data-driven efficiency modeling and analysis of all-electric ship powertrain: A comparison of power system architectures," *IEEE Trans. Transport. Electrific.*, vol. 8, no. 2, pp. 1930–1943, Jun. 2022.

[25] L. Xu et al., "A review of DC shipboard microgrids-part 1: Power architectures, energy storage, and power converters," *IEEE Trans. Power Electron.*, vol. 37, no. 5, pp. 5155–5172, May 2022.

[26] S. Qazi et al., "Powering maritime: Challenges and prospects in ship electrification," *IEEE Electrific. Mag.*, vol. 11, no. 2, pp. 74–87, Jun. 2023.

[27] W. N. Ayers, "DC grids for ship propulsion: Benefits and challenges," in *Proc. 2022 SNAME Maritime Conv.*, Sep. 2022, pp. 1–25.

[28] K. Kim, K. Park, G. Roh, and K. Chun, "DC-grid system for ships: A study of benefits and technical considerations," *J. Int. Maritime Saf., Environ. Affairs, Shipping*, vol. 2, no. 1, pp. 1–12, Nov. 2018.

[29] L. Qi and J. Lindtjørn, "DC marine vessel electric system design with case studies," *Medium Voltage DC Syst. Architectures*, vol. 143, Ch. 10, pp. 303–350, 2021.

[30] N. Doerry and K. McCoy, "Next generation integrated power system: NGIPS technology development roadmap:," Defense Tech. Inf. Center, Fort Belvoir, VA, Tech. Rep., Nov. 2007.

[31] A. Latorre, T. B. Soeiro, R. Geertsma, A. Coraddu, and H. Polinder, "Shipboard DC systems: A critical overview: Challenges in primary distribution, power-electronics-based protection, and power scalability," *IEEE Open J. Ind. Electron. Soc.*, vol. 4, pp. 259–286, 2023.

[32] L. Xu et al., "A review of DC shipboard microgrids-part II: Control architectures, stability analysis, and protection schemes," *IEEE Trans. Power Electron.*, vol. 37, no. 4, pp. 4105–4120, Apr. 2022.

[33] N. Zohrabi, J. Shi, and S. Abdelwahed, "An overview of design specifications and requirements for the MVDC shipboard power system," *Int. J. Elect. Power Energy Syst.*, vol. 104, pp. 680–693, Jan. 2019.

[34] *IEEE Recommended Practice for 1 kV to 35 kV Medium-Voltage DC Power Systems on Ships*, IEEE Std 1709-2018 (Revision of IEEE Std 1709-2010), pp. 1–54, 2018.

[35] R. M. Cuzner and D. A. Esmaili, "Fault tolerant shipboard MVDC architectures," in *Proc. 2015 Int. Conf. Elect. Syst. Aircraft, Railway, Ship Propulsion Road Veh.*, Mar. 2015, pp. 1–6.

[36] V. Staudt, R. Bartelt, and C. Heising, "Short-circuit protection issues in DC ship grids," in *Proc. 2013 IEEE Electric Ship Technol. Symp.*, Arlington, VA, USA, Apr. 2013, pp. 475–479.

[37] M. Babaei, J. Shi, and S. Abdelwahed, "A survey on fault detection, isolation, and reconfiguration methods in electric ship power systems," *IEEE Access*, vol. 6, pp. 9430–9441, 2018.

[38] Y. Song and B. Wang, "Survey on reliability of power electronic systems," *IEEE Trans. Power Electron.*, vol. 28, no. 1, pp. 591–604, Jan. 2013.

[39] I. Baylakoglu et al., "The detrimental effects of water on electronic devices," *ePrime - Adv. Electr. Eng., Electron. Energy*, vol. 1, 2021, Art. no. 100016.

[40] P. R. Thies, G. H. Smith, and L. Johanning, "Addressing failure rate uncertainties of marine energy converters," *Renewable Energy*, vol. 44, pp. 359–367, Aug. 2012.

[41] S. Peyghami, P. Palensky, and F. Blaabjerg, "An overview on the reliability of modern power electronic based power systems," *IEEE Open J. Power Electron.*, vol. 1, pp. 34–50, 2020.

[42] S. B. Aruna, D. Suchitra, R. Rajarajeswari, and S. G. Fernandez, "A comprehensive review on the modern power system reliability assessment," *Int. J. Renewable Energy Res.*, Dec., vol. 11, no. 4, pp. 1734–1747, 2021.

[43] A. Altamimi and D. Jayaweera, "Reliability of power systems with climate change impacts on hierarchical levels of PV systems," *Electric Power Syst. Res.*, vol. 190, 2021, Art. no. 106830.

[44] H. Mahdi, B. Hoff, and T. Ostrem, "A review of power converters for ships electrification," *IEEE Trans. Power Electron.*, vol. 38, no. 4, pp. 4680–4697, Apr. 2023.

[45] D. Kumar and F. Zare, "A comprehensive review of maritime microgrids: System architectures, energy efficiency, power quality, and regulations," *IEEE Access*, vol. 7, pp. 67249–67277, 2019.

[46] T. Longva, "Maritime forecast to 2050," DNV-GL Region North Europe, Tech. Rep., 2020.

[47] M. Svanberg, J. Ellis, J. Lundgren, and I. Landalv, "Renewable methanol as a fuel for the shipping industry," *Renewable Sustain. Energy Rev.*, vol. 94, pp. 1217–1228, Oct. 2018.

[48] S. Atilhan, S. Park, M. M. El-Halwagi, M. Atilhan, M. Moore, and R. B. Nielsen, "Green hydrogen as an alternative fuel for the shipping industry," *Curr. Opin. Chem. Eng.*, vol. 31, Mar. 2021, Art. no. 100668.

[49] DNV-GL, "Ammonia as a marine fuel," Group Technology & research DNV, White paper, 2020.

[50] *IEEE Recommended Practice for Electrical Installations on Shipboard-Design*," IEEE Std 45.1-2023, 2023, pp. 1–238.

[51] "Electrical installations in ships - part 201: System design - general," *IEC 60092-201:2019*, pp. 1–42, 2019.

[52] "Electrical installations in ships - part 202: System design - protection," *IEC 60092-202:2016*, pp. 1–19, 2016.

[53] "Electrical installations in ships - primary dc distribution - system design architecture," IEC 63108:2017, pp. 1–20, 2017.

[54] M. Andrus, M. Bosworth, J. Crider, H. Ouroua, E. Santi, and S. Sudhoff, "Notional system report," Electric Ship Res. Develop. Consortium, Tech. Rep., 2014.

[55] ESRDC, "Model description document notional four zone MVDC shipboard power system model," Electric Ship Res. Develop. Consortium, Tech. Rep. DCN 43-7281-20, 2020.

[56] R. van der Sande, R. Deshmukh, A. Shekhar, and P. Bauer, "DC link capacity enhancement for MMC-based distribution link using dynamic voltage operation," in *Proc. 11th Int. Conf. Power Electron. ECCE Asia*, 2023, pp. 636–642.

[57] E. Rodriguez-Diaz, F. Chen, J. C. Vasquez, J. M. Guerrero, R. Burgos, and D. Boroyevich, "Voltage-level selection of future two-level LVdc distribution grids: A compromise between grid compatibiliy, safety, and efficiency," *IEEE Electrific. Mag.*, vol. 4, no. 2, pp. 20–28, Jun. 2016.

[58] M. Di Piazza, M. Luna, G. La Tona, M. Pucci, A. Accetta, and A. Pietra, "A new method for selecting the voltage level for an advantageous transition to DC distribution in ships," in *Proc. 2018 IEEE Int. Conf. Elect. Syst. Aircr., Railway, Ship Propulsion Road Veh. Int. Transp. Electrific. Conf.*, Nov. 2018, pp. 1–5.

[59] M. Ahmadi, A. Shekhar, and P. Bauer, "Switch voltage rating selection considering cost- oriented redundancy and modularity-based trade-offs in modular multilevel converter," *IEEE Trans. Power Del.*, vol. 38, no. 4, pp. 2831–2842, Aug. 2023.

[60] R. M. Cuzner, R. Soman, M. M. Steurer, T. A. Toshon, and M. O. Faruque, "Approach to scalable model development for navy shipboard compatible modular multilevel converters," *IEEE Trans. Emerg. Sel. Topics Power Electron.*, vol. 5, no. 1, pp. 28–39, Mar. 2017.

[61] D. Ronanki and S. S. Williamson, "Modular multilevel converters for transportation electrification: Challenges and opportunities," *IEEE Trans. Transport. Electrific.*, vol. 4, no. 2, pp. 399–407, Jun. 2018.

[62] S. Yadav, Z. Qin, and P. Bauer, "Bipolar DC grids on ships: Possibilities and challenges," *e & i Elektrotechnik und Informationstechnik*, vol. 139, no. 4, pp. 458–467, Aug. 2022.

[63] Z. Jin, G. Sulligoi, R. Cuzner, L. Meng, J. C. Vasquez, and J. M. Guerrero, "Next-generation shipboard DC power system: Introduction smart grid and DC microgrid technologies into maritime electrical netowrks," *IEEE Electrific. Mag.*, vol. 4, no. 2, pp. 45–57, Jun. 2016.

[64] D. Kumar, F. Zare, and A. Ghosh, "DC microgrid technology: System architectures, AC grid interfaces, grounding schemes, power quality, communication networks, applications, and standardizations aspects," *IEEE Access*, vol. 5, pp. 12230–12256, 2017.

[65] O. Husev and D. Vinnikov, "DC microgrid: State of art, driving force, challenges and perspectives," *Stud. Syst., Decis. Control*, vol. 512, pp. 149–190, 2023.

[66] T. R. De Oliveira, A. S. Bolzon, and P. F. Donoso-Garcia, "Grounding and safety considerations for residential DC microgrids," in *Proc. IECON 2014-40th Annu. Conf. IEEE Ind. Electron. Soc.*, Dallas, TX, USA, Oct. 2014, pp. 5526–5532.

[67] S. Rivera, R. Lizana F, S. Kouro, T. Dragicevic, and B. Wu, "Bipolar DC power conversion: State-of-the-art and emerging technologies," *IEEE Trans. Emerg. Sel. Topics Power Electron.*, vol. 9, no. 2, pp. 1192–1204, Apr. 2021.

[68] S. D. Tavakoli, P. Zhang, X. Lu, and M. Hamzeh, "Mutual interactions and stability analysis of bipolar DC microgrids," *CSEE J. Power Energy Syst.*, vol. 5, no. 4, pp. 444–453, Dec. 2019.

[69] R. W. Revie, *Corrosion and Corrosion Control: An Introduction to Corrosion Science and Engineering*. Hoboken, NJ, USA: Wiley, 2008.

[70] S. A. Memon and P. Fromme, "Stray current corrosion and mitigation: A synopsis of the technical methods used in DC transit systems," *IEEE Electrific. Mag.*, vol. 2, no. 3, pp. 22–31, Sep. 2014.

[71] M. Pourmirasghariyan, S. F. Zarei, and M. Hamzeh, "DC-system grounding: Existing strategies, performance analysis, functional characteristics, technical challenges, and selection criteria - A review," *Electric Power Syst. Res.*, vol. 206, May 2022, Art. no. 107769. [Online]. Available: https://www.sciencedirect.com/science/article/pii/S0378779621007501

[72] J. Mohammadi, F. B. Ajaei, and G. Stevens, "DC microgrid grounding strategies," in *Proc. IEEE/IAS 54th Ind. Commercial Power Syst. Tech. Conf.*, May 2018, pp. 1–6.

[73] J. Mohammadi, F. Badrkhani Ajaei, and G. Stevens, "Grounding the DC microgrid," *IEEE Trans. Ind. Appl.*, vol. 55, no. 5, pp. 4490–4499, Sep./Oct. 2019.

[74] Koninklijk Nederlands Normalisatie Instituut (NEN), "DC installations for low voltage," in *NPR 9090:2024, Koninklijk Nederlands Normalisatie Institute*, Delft, The Netherlands, 2024.

[75] A. Blinov, I. Roasto, A. Chub, P. Emiliani, and D. Vinnikov, "Electric power management and control in DC buildings state-of-the-art and emerging technologies," *Power Quality: Infrastructures Control*, pp. 67–96, 2023.

[76] X. Yu, X. Wang, Y. Hu, T. Niu, B. Hu, and K. Xie, "Effect of relative humidity on reliability of wind power converter and its application to wind farm reliability evaluation," in *Proc. 4th Int. Conf. Energy, Electr. Power Eng.*, Apr. 2021, pp. 470–475.

[77] B. Stevens and S. Santoso, "Reliability analysis of a shipboard electrical power distribution system based on breaker-and-a-half topology," in *Proc. 2013 IEEE Electric Ship Technol. Symp.*, Apr. 2013, pp. 387–393.

[78] A. Shekhar, L. Ramirez-Elizondo, and P. Bauer, "DC microgrid islands on ships," in *Proc. IEEE 2nd Int. Conf. DC Microgrids*, Jun. 2017, pp. 111–118.

[79] F. D. Kanellos, G. J. Tsekouras, and J. Prousalidis, "Onboard DC grid employing smart grid technology: Challenges, state of the art and future prospects," *IET Elect. Syst. Transp.*, vol. 5, no. 1, pp. 1–11, 2015.

[80] O. Simmonds, "DC: Is it the alternative choice for naval power distribution?," *J. Mar. Eng. Technol.*, vol. 13, no. 3, pp. 37–43, Dec. 2014.

[81] S. O. Settemsdal, E. Haugan, K. Aagesen, B. Zahedi, and S. Drilling, "New enhanced safety power plant solution for DP vessels operated in closed ring configuration," in *Proc. Dyn. Positioning Conf.*, 2014, pp. 1–21.

[82] U. Javaid, D. Dujic, and W. Van Der Merwe, "MVDC marine electrical distribution: Are we ready?," in *Proc. IECON - 41st Annu. Conf. IEEE Ind. Electron. Soc.*, Nov. 2015, pp. 823–828.

[83] J. Newell, D. Mattick, and C. Hodge, "The electric warship IV," *Trans. IMarE*, vol. 111, pp. 25–40, 1999.

[84] N. Doerry, "Naval power systems: Integrated power systems for the continuity of the electrical power supply," *IEEE Electrific. Mag.*, vol. 3, no. 2, pp. 12–21, Jun. 2015.

[85] A. Adnanes, "Maritime electrical installations and diesel electric propulsion," pp. 1–81, ABB, Tech. Rep., 2003.

[86] American Bureau of Shipping, "Guide for dynamic positioning systems," ABS, Tech. Rep., 2021.

[87] J. Schuddebeurs, C. Booth, G. Burt, and J. McDonald, "Impact of marine power system architectures on IFEP vessel availability and survivability," in *Proc. 2007 IEEE Electric Ship Technol. Symp.*, May 2007, pp. 14–21.

[88] M. Othman, A. Anvari-Moghaddam, and J. M. Guerrero, "Hybrid shipboard microgrids: System architectures and energy management aspects," in *Proc. IECON - 43rd Annu. Conf. IEEE Ind. Electron. Soc.*, Oct. 2017, pp. 6801–6806.

[89] M. U. Mutarraf et al., "Adaptive power management of hierarchical controlled hybrid shipboard microgrids," *IEEE Access*, vol. 10, pp. 21397–21411, 2022.

[90] P. M. Kishore and R. Bhimasingu, "Enabling the fault tolerant operation of shipboard microgrid architecture," in *Proc. 1st Int. Conf. Sustain. Green Buildings Communities*, Dec. 2016, pp. 1–5.

[91] C. R. Petry and J. W. Rumburg, "Zonal electrical distribution systems: An affordable architecture for the future," *Nav. Eng. J.*, vol. 105, no. 3, pp. 45–51, May 1993.

[92] H. Hegner and B. Desai, "Integrated fight through power," in *Proc. IEEE Power Eng. Soc. Summer Meeting*, Jul. 2002, pp. 336–339.

[93] M. B. Stevens and S. Santoso, "Improving the reliability of breaker-and-a-half substations using sectionalized busbars," in *Proc. IEEE Power Energy Soc. Gen. Meeting*, Jul. 2013, pp. 1–5.

[94] J. S. Chalfant and C. Chryssostomidis, "Analysis of various all-electric-ship electrical distribution system topologies," in *Proc. 2011 IEEE Electric Ship Technol. Symp.*, Apr. 2011, pp. 72–77.

[95] D. Cahyagi and E. Koenhardono, "Study of shipboard power distribution system: Review on an aplication of AC zonal distribution," *IPTEK J. Eng.*, vol. 4, pp. 1–6, 2018.

[96] N. H. Doerry and J. C. Davis, "Integrated power system for marine applications," *Nav. Eng. J.*, vol. 106, no. 3, pp. 77–90, May 1994.

[97] J. Ciezki and R. Ashton, "Selection and stability issues associated with a navy shipboard DC zonal electric distribution system," *IEEE Trans. Power Del.*, vol. 15, no. 2, pp. 665–669, Apr. 2000.

[98] P. P. Irene, A. Kurniawan, and E. S. Koenhardono, "Load flow analysis due to reconfiguration of AC to DC electrical distribution system on Trailing Suction Hopper Dredger (TSHD) vessel," in *Proc. 2022 Int. Conf. Elect. Inf. Technol.*, Sep. 2022, pp. 276–281.

[99] G. Chang, Y. Wu, S. Shao, Z. Huang, and T. Long, "DC bus systems for electrical ships: Recent advances and analysis of a real case," *IEEE Electrific. Mag.*, vol. 8, no. 3, pp. 28–39, Sep. 2020.

[100] S. Jothibasu and S. Santoso, "New electric shipboard topologies for high resiliency," *IEEE Trans. Power Syst.*, vol. 33, no. 3, pp. 2975–2983, May 2018.

[101] Q. Xu, Y. Xu, P. Tu, T. Zhao, and P. Wang, "Systematic reliability modeling and evaluation for on-board power systems of more electric aircrafts," *IEEE Trans. Power Syst.*, vol. 34, no. 4, pp. 3264–3273, Jul. 2019.

[102] M. Y. Nguyen and Y. T. Yoon, "A comparison of microgrid topologies considering both market operations and reliability," *Electric Power Compon. Syst.*, vol. 42, no. 6, pp. 585–594, Apr. 2014. [Online]. Available: https://doi.org/10.1080/15325008.2014.880963

[103] A. Haxhiu, A. Abdelhakim, S. Kanerva, and J. Bogen, "Electric power integration schemes of the hybrid fuel cells and batteries-fed marine vessels - an overview," *IEEE Trans. Transport. Electrific.*, vol. 8, no. 2, pp. 1885–1905, Jun. 2022.

[104] B. Zahedi, L. E. Norum, and K. B. Ludvigsen, "Optimized efficiency of all-electric ships by DC hybrid power systems," *J. Power Sources*, vol. 255, pp. 341–354, Jun. 2014.

[105] G. J. Tsekouras and F. D. Kanellos, "Ship to shore connection - reliability analysis of ship power system," in *Proc. 22nd Int. Conf. Elect. Mach.*, Sep. 2016, pp. 2955–2961.

[106] H. Jeon, K. Park, and J. Kim, "Comparison and verification of reliability assessment techniques for fuel cell-based hybrid power system for ships," *J. Mar. Sci. Eng.*, vol. 8, no. 2, Feb., Art. no. 74.

[107] S. Karimi, M. Zadeh, and J. A. Suul, "A multilayer framework for reliability assessment of shore-to-ship fast charging system design," *IEEE Trans. Transport. Electrific.*, vol. 8, no. 3, pp. 3028–3040, Sep. 2022.

[108] R. Billinton and R. N. Allan, *Reliability Evaluation of Engineering Systems*. Berlin, Germany: Springer, 1992.

[109] R. N. Allan et al. *Reliability Evaluation of Power Systems*. Berlin, Germany: Springer, 2013.

[110] R. Allan and R. Billinton, "Probabilistic methods applied to electric power systems-are they worth it?," *Power Eng. J.*, vol. 6, no. 3, pp. 121–129, May 1992.

[111] D. O. Koval et al., "IEEE recommended practice for the design of reliable industrial and commercial power systems," *IEEE Std 493-2007*, 2007, doi: 10.1109/IEEESTD.2007.380668.

[112] N. H. Doerry and J. V. Amy, "Implementing quality of service in shipboard power system design," in *Proc. 2011 IEEE Electric Ship Technol. Symp.*, Apr. 2011, pp. 1–8.

[113] B. W. Tuinema, J. R. Torres, A. I. Stefanov, F. M. Gonzalez-Longatt, and M. Van Der Meijden, *Probabilistic Reliability Analysis of Power Systems*. Berlin, Germany: Springer, 2020.

[114] N. Doerry, "Designing electrical power systems for survivability and quality of service," *Nav. Eng. J.*, vol. 119, no. 2, pp. 25–34, Oct. 2007.

[115] N. Doerry and D. Clayton, "Shipboard electrical power quality of service," in *Proc. Electric Ship Technol. Symp.* Aug. 2005, pp. 274–279.

[116] M. Al-Kuwaiti, N. Kyriakopoulos, and S. Hussein, "A comparative analysis of network dependability, fault-tolerance, reliability, security, and survivability," *IEEE Commun. Surv. Tut.*, vol. 11, no. 2, pp. 106–124, Second Quarter 2009.

[117] I. Bolvashenkov, J. Kammermann, I. Frenkel, and H.-G. Herzog, "Multi-level hierarchical reliability model of technical systems: Theory and application," *Adv. Rel. Anal. Appl.*, vol. 1, pp. 201–234, 2020.

[118] R. Billinton and R. Allan, "Power-system reliability in perspective," *Electron. Power*, vol. 30, no. 3, pp. 231–236, Mar. 1984.

[119] S. Peyghami, Z. Wang, and F. Blaabjerg, "A guideline for reliability prediction in power electronic converters," *IEEE Trans. Power Electron.*, vol. 35, no. 10, pp. 10958–10968, Oct. 2020. [Online]. Available: https://ieeexplore.ieee.org/document/9042353/?arnumber=9042353&tag=1

[120] S. Peyghami, P. Palensky, M. Fotuhi-Firuzabad, and F. Blaabjerg, "System-level design for reliability and maintenance scheduling in modern power electronic-based power systems," *IEEE Open Access J. Power Energy*, vol. 7, pp. 414–429, 2020. [Online]. Available: https://ieeexplore.ieee.org/abstract/document/9214842

[121] S. Peyghami, F. Blaabjerg, and P. Palensky, "Incorporating power electronic converters reliability into modern power system reliability analysis," *IEEE Trans. Emerg. Sel. Topics Power Electron.*, vol. 9, no. 2, pp. 1668–1681, Apr. 2021.

[122] S. Peyghami, Z. Wang, and F. Blaabjerg, "Reliability modeling of power electronic converters: A general approach," in *Proc. 20th Workshop Control Model. Power Electron.*, Toronto, ON, Canada, 2019, pp. 1–7.

[123] United States Dept. of Defense, "Military Handbook-Reliability Prediction of Electronic Equipment," *MIL HDBK 217F*, vol. 2, pp. 1–205, 1995.

[124] IEC, "Reliability data handbook-universal model for reliability prediction of electronics components, PCBs and equipment," *IEC TR 62380*, 2004.

[125] Institute pour la Maitrise des Risques, "Reliability methodology for electronic systems," *FIDES Guide 2022*, vol. A, pp. 1–498, 2023.

[126] R. Bayerer, T. Herrmann, T. Licht, J. Lutz, and M. Feller, "Model for power cycling lifetime ofIGBT modules-various factors influencing lifetime," in *Proc. 5th Int. Conf. Integr. Power Electron. Syst.*, 2008, pp. 1–6.

[127] R. R. Errabelli and P. Mutschler, "Fault-tolerant voltage source inverter for permanent magnet drives," *IEEE Trans. Power Electron.*, vol. 27, no. 2, pp. 500–508, Feb. 2012.

[128] L. R. Gopireddy, L. M. Tolbert, and B. Ozpineci, "Power cycle testing of power switches: A literature survey," *IEEE Trans. Power Electron.*, vol. 30, no. 5, pp. 2465–2473, May 2015.

[129] U.-M. Choi, S. Jorgensen, and F. Blaabjerg, "Advanced accelerated power cycling test for reliability investigation of power device modules," *IEEE Trans. Power Electron.*, vol. 31, no. 12, pp. 8371–8386, Dec. 2016.

[130] A. Dubey and S. Santoso, "A two-level topology design framework for reliable shipboard power systems," *Inventions*, vol. 1, no. 3, Sep. 2016, Art. no. 14.

[131] R. E. Brown, "Failure rate modeling using equipment inspection data," in *Proc. IEEE Power Eng. Soc. Gen. Meeting*, 2004, pp. 693–700.

[132] Y.-C. Wu and W.-F. Chang, "A study on optimal reliability indices in an electrical distribution system," in *Proc. 2000 Int. Conf. Power Syst. Technol.*, 2000, vol. 2, pp. 727–732.

[133] R. E. Brown and J. R. Ochoa, "Distribution system reliability: Default data and model validation," *IEEE Trans. Power Syst.*, vol. 13, no. 2, pp. 704–709, May 1998.

[134] B. Amanulla, S. Chakrabarti, and S. N. Singh, "Reconfiguration of power distribution systems considering reliability and power loss," *IEEE Trans. Power Del.*, vol. 27, no. 2, pp. 918–926, Apr. 2012.

[135] DNV-GL, "Rules classification: Ships," Additional class notations (Pt. 6) - Propulsion, power generation and auxiliary systems (Ch. 2), 2024.

[136] S. Kanerva and J.-F. Hansen, "State of the art in electric propulsion - viewpoint on redundancy," in *Proc. 2009 IEEE Electric Ship Technol. Symp.*, Apr. 2009, pp. 499–504.

[137] W. Li et al. *Reliability Assessment of Electric Power Systems Using Monte Carlo Methods*. Berlin, Germany: Springer, 2013.

[138] R. Menis, A. da Rin, A. Vicenzutti, and G. Sulligoi, "All electric ships dependable design: Integrated power system analysis using dynamic reliability block diagram," in *Proc. Mar. Elect. Control Syst. Saf. Conf.*, 2013, pp. 1–7.

[139] R. Bleilevens, J. Priebe, N. Wehbring, and A. Moser, "Reliability analysis of DC distribution grids," in *Proc. 54th Int. Universities Power Eng. Conf.*, Sep. 2019, pp. 1–6.

[140] G. Li et al., "Feasibility and reliability analysis of LCC DC grids and LCC/VSC hybrid DC grids," *IEEE Access*, vol. 7, pp. 22445–22456, 2019.

[141] A. Hoyland and M. Rausand, *System Reliability Theory: Models and Statistical Methods*. Hoboken, NJ, USA: Wiley, 2009.

[142] Z. Wang, S. Karimi, M. Zadeh, and M. Heimdal, "Reliability modelling of marine hybrid power and propulsion system considering operation profile," in *Proc. 2023 IEEE Int. Conf. Elect. Syst. Aircraft, Railway, Ship Propulsion Road Veh. Int. Transp. Electrific. Conf.*, Venice, Italy, Mar. 2023, pp. 1–6.

[143] W. Du, "Reliability evaluation of a zonal shipboard power system based on minimal cut set," in *Proc. Adv. Swarm Intell. 7th Int. Conf.*, 2016, pp. 563–572.

[144] R. Allan, R. Billinton, and M. De Oliveira, "An efficient algorithm for deducing the minimal cuts and reliability indices of a general network configuration," *IEEE Trans. Rel.*, vol. R-25, no. 4, pp. 226–233, Oct. 1976.

[145] A. Dubey and S. Santoso, "Availability-based distribution circuit design for shipboard power system," *IEEE Trans. Smart Grid*, vol. 8, no. 4, pp. 1599–1608, Jul. 2017.

[146] A. Vicenzutti, R. Menis, and G. Sulligoi, "All-electric ship-integrated power systems: Dependable design based on fault tree analysis and dynamic modeling," *IEEE Trans. Transport. Electrific.*, vol. 5, no. 3, pp. 812–827, Sep. 2019.

[147] H. Jiang, C. H. Peng, and J. Xiao, "Reliability analysis for the power system of the nuclear ship Savannah," *J. Phys.: Conf. Ser.*, vol. 2208, no. 1, Mar. 2022, Art. no. 012003.

[148] A. Dubey, S. Santoso, and A. Arapostathis, "Reliability analysis of three-dimensional shipboard electrical power distribution systems," in *Proc. 2015 IEEE Electric Ship Technol. Symp.*, Jun. 2015, pp. 93–98.

[149] M. Novak, A. Sangwongwanich, and F. Blaabjerg, "Monte Carlo-based reliability estimation methods for power devices in power electronics systems," *IEEE Open J. Power Electron.*, vol. 2, pp. 523–534, 2021.

[150] P. O'Connor and A. Kleyner," in *Practical Reliability Engineering*. Hoboken, NJ, USA: Wiley, 2012.

[151] F. M. Dekking, C. Kraaikamp, H. P. Lopuhaä, and L. E. Meester," in *A Modern Introduction to Probability and Statistics: Understanding Why and How*. Berlin, Germany: Springer, 2005.

[152] B. Zhang, M. Wang, and W. Su, "Reliability analysis of power systems integrated with high-penetration of power converters," *IEEE Trans. Power Syst.*, vol. 36, no. 3, pp. 1998–2009, May 2021.

[153] A. Rei and M. Schilling, "Reliability assessment of the Brazilian power system using enumeration and Monte Carlo," *IEEE Trans. Power Syst.*, vol. 23, no. 3, pp. 1480–1487, Aug. 2008.

[154] N. Shahidirad, M. Niroomand, and R.-A. Hooshmand, "Investigation of PV power plant structures based on Monte Carlo reliability and economic analysis," *IEEE J. Photovolt.*, vol. 8, no. 3, pp. 825–833, May 2018. [Online]. Available: https://ieeexplore.ieee.org/document/8334818/

[155] A. Sankarakrishnan and R. Billinton, "Sequential Monte Carlo simulation for composite power system reliability analysis with time varying loads," *IEEE Trans. Power Syst.*, vol. 10, no. 3, pp. 1540–1545, Aug. 1995.

[156] C. Singh, T. P. Chander, and J. Feng, "Convergence characteristics of two Monte Carlo models for reliability evaluation of interconnected power systems," *Electric Power Syst. Res.*, vol. 28, no. 1, pp. 1–9, Oct. 1993.

[157] H. Patel and A. Deshpande, "Reliability evaluation of power system using Monte Carlo simulation in PSPICE," *Int. J. Appl. Eng. Res.*, vol. 14, no. 9, pp. 2252–2259, 2019.

[158] D. Siemaszko and S. Pittet, "Impact of modularity and redundancy in optimising the reliability of power systems that include a large number of power converters," *Microelectronics Rel.*, vol. 51, no. 9, pp. 1484–1488, Sep. 2011.

[159] S. Eriksen and M. Lutzen, "The impact of redundancy on reliability in machinery systems on unmanned ships," *WMU J. Maritime Affairs*, vol. 21, no. 2, pp. 161–177, Jun. 2022. [Online]. Available: https://doi.org/10.1007/s13437-021-00259-7

[160] A. Zhaksylyk, M. M. Hasan, S. Chakraborty, T. Geury, and O. Hegazy, "Effects of modularity on the performance and reliability of SiC MOSFET-based active front-end rectifiers in EV charging application," in *Proc. IECON - 48th Annu. Conf. IEEE Ind. Electron. Soc.*, Brussels, Belgium, Oct. 2022, pp. 1–7.

[161] S. Mousavizadeh, T. G. Bolandi, M.-R. Haghifam, M. Moghimi, and J. Lu, "Resiliency analysis of electric distribution networks: A new approach based on modularity concept," *Int. J. Elect. Power Energy Syst.*, vol. 117, May 2020, Art. no. 105669.

[162] K. C. Nagaraj, J. Carroll, T. Rosenwinkel, A. Arapostathis, M. Grady, and E. J. Powers, "Perspectives on power system reconfiguration for shipboard applications," in *Proc. 2007 IEEE Electric Ship Technol. Symp.*, Arlington, VA, USA, May 2007, pp. 188–195.

[163] R. S. Rao, K. Ravindra, K. Satish, and S. V. L. Narasimham, "Power loss minimization in distribution system using network reconfiguration in the presence of distributed generation," *IEEE Trans. Power Syst.*, vol. 28, no. 1, pp. 317–325, Feb. 2013.

[164] M. Guimaraes, J. Lorenzeti, and C. Castro, "Reconfiguration of distribution systems for stability margin enhancement using tabu search," in *Proc. 2004 Int. Conf. Power Syst. Technol.*, 2004, vol. 2, pp. 1556–1561.

[165] L. Agnello, M. Cossentino, G. D. Simone, and L. Sabatucci, "Shipboard power systems reconfiguration: A compared analysis of state-of-the-art approaches," in *Proc. Smart Ship Technol. Int. Conf.*, 2017, pp. 1–9.

[166] O. Badran, S. Mekhilef, H. Mokhlis, and W. Dahalan, "Optimal reconfiguration of distribution system connected with distributed generations: A review of different methodologies," *Renewable Sustain. Energy Rev.*, vol. 73, pp. 854–867, Jun. 2017. [Online]. Available: https://www.sciencedirect.com/science/article/pii/S1364032117302101

[167] P. Mitra and G. K. Venayagamoorthy, "Implementation of an intelligent reconfiguration algorithm for an electric ship's power system," *IEEE Trans. Ind. Appl.*, vol. 47, no. 5, pp. 2292–2300, Sep./Oct. 2011. [Online]. Available: https://ieeexplore.ieee.org/document/5958603/

[168] L. Ouyang, Y. Li, Y. Tan, J. Xiao, and Y. Cao, "Reconfiguration optimization of DC zonal distribution network of shipboard power system," in *Proc. 2016 IEEE Transp. Electrific. Conf. Expo, Asia-Pacific*, Jun. 2016, pp. 444–448.

[169] S. Srivastava and K. Butler-Purry, "A pre-hit probabilistic reconfiguration methodology for shipboard power systems," in *Proc. IEEE Electric Ship Technol. Symp.*, 2005, pp. 99–104.

[170] Y. Zhang, R. Wu, F. Iannuzzo, and H. Wang, "Aging investigation of the latest standard dual power modules using improved interconnect technologies by power cycling test," *Microelectronics Rel.*, vol. 138, Nov. 2022, Art. no. 114740.

ROBIN VAN DER SANDE (Student Member, IEEE) received the B.Sc. degree in electrical engineering (*cum laude*) and the M.Sc. degree in electrical power engineering (*cum laude*) from the Delft University of Technology, Delft, The Netherlands, in 2020 and 2022, respectively. He is currently working toward the Ph.D. degree in electrical engineering with the dc Systems, Energy Conversion and Storage Group as part of the Electrical Sustainability Energy Department with TU Delft, Delft, The Netherlands.

He is a Guest Researcher with the Netherlands Defense Academy, Den Helder, The Netherlands. With his Ph.D. project, he addresses the reliability and survivability aspects of dc shipboard power systems from the system design perspective to improve the availability and fault tolerance of future all-electric ships. His research interests include ship electrification, the reliability and survivability of power systems, and modular multilevel converters.

ADITYA SHEKHAR (Member, IEEE) received the bachelor's degree (Hons.) in electrical from the National Institute of Technology, Surat, India, in 2010, and the M.Sc. (cum laude) and Ph.D. degrees in electrical engineering from the Delft University of Technology, Delft, The Netherlands, in 2015 and 2020, respectively.

He worked as a Postdoctoral on EU projects, such as Trolley 2.0, OSCD and EASY-RES. He has authored and coauthored more than 20 Journals, 50 international conference papers, and 2 book chapters on several research topics, such as reliable power electronics, capacity-enhanced medium voltage dc grids, trolley grids, smart charging of electric vehicles, modular multilevel converters, partial discharges in cables, series arc protection, wireless EV charging and solar roads. He is an Assistant Professor in the field of Reliable Power Electronic Systems at Delft University of Technology and developed the Power Electronics and Reliability Lab (The PEARL), where the robustness of power electronic systems is tested. He obtained research grants as part of several national and international consortiums such as PowerizeD (EU-Horizon), Sunrise (EU-Twinning), Survivable DC Power Systems for Ships (Dutch research council; NWO-KIC) and works with a team of 7 Phd students to explore research on reliable power electronic systems.

Dr. Shekhar has also contributes to the Student and Young Professionals Committee of the IEEE Industrial Electronics Society in travel grant reviews and its promotional activities.

PAVOL BAUER (Senior Member, IEEE) received the master's degree in electrical engineering from the Technical University of Kosice, Koice, Slovakia, in 1985 and the Ph.D. degree from the Delft University of Technology, Delft, The Netherlands, in 1995.

He is currently a Full Professor with the Department of Electrical Sustainable Energy, Delft University of Technology, where he is the Head of the DC systems, Energy Conversion, and Storage Group. He is also an Honorary Professor with the Politehnica University, Timisoara, Romania. From 2002 to 2003, he was with KEMA (DNV GL), Arnhem, on different projects related to power electronics applications in power systems. He published more than 180 journal and 450 conference papers in his field (with H factor Google Scholar 65, Web of Science 45) and eight books, ten international patents, and organized several tutorials at international conferences. He has worked on many projects for the industry concerning wind and wave energy, power electronic applications for power systems such as Smarttrafo, as well as HVDC systems, and projects for smart cities such as photovoltaic (PV) charging of electric vehicles, PV and storage integration, and contactless charging. He participated in several Leonardo da Vinci, H2020, and Electric Mobility Europe EU Projects as Project Partner (ELINA, INETELE, E-Pragmatic, Micact, Trolly 2.0, OSCD, P2P, Progressus, Tulip, and Flow) and a coordinator (PEMCWebLab.com-Edipe, SustEner, Eranet, and DCMICRO). His research interests include power electronics for charging electric vehicles and DC grids.

Dr. Bauer was the recipient of the title Professor from the President of Czech Republic with the Brno University of Technology, Brno, Czechia in 2008, and with the Delft University of Technology in 2016, and the Honorary Doctorate from Politehnica University. He is the Former Chairman of Benelux IEEE Joint Industry Applications Society, Power Electronics Society, and Power Engineering Society Chapter, the Chairman of the Power Electronics and Motion Control Council, a Member of the Executive Committee of the European Power Electronics Association, and a Member of the International Steering Committee at numerous conferences.